metals

MDPI

Review

From Conventional Dispersion Strengthening to Core–Shell Reinforcement Architectures in Iron-Based Metal Matrix Composites: A Review

Petr M. Korusenko [1,*], Vladimir K. Kudymov [1], Vladimir E. Gaishun [2] and Elena G. Zemtsova [1]

[1] Institute of Chemistry, St. Petersburg State University, 7-9 Universitetskaya Emb., 199034 Saint Petersburg, Russia; ezimtsova@yandex.ru (E.G.Z.)
[2] Faculty of Physics and Information Technologies, Francisk Skorina Gomel State University, Sovetskaya 104, 246019 Gomel, Belarus
* Correspondence: korusenko_petr@mail.ru or p.korusenko@spbu.ru

Abstract

Despite extensive research on iron-based metal matrix composites (Fe-based MMCs), an integrated assessment linking fabrication methods, reinforcement architectures, interface engineering, and strengthening mechanisms remains limited. This review summarizes recent advances in Fe-based MMCs, with emphasis on the relationships among processing routes, microstructural evolution, reinforcement characteristics, and mechanical performance. Powder metallurgy, casting, and additive manufacturing are critically compared in terms of their processing characteristics, advantages, limitations, and suitability for iron-based systems. The effects of reinforcement size, morphology, distribution, and volume fraction on composite performance are discussed. Particular attention is given to interface engineering strategies and architectured core–shell reinforcements produced through in situ reactions and solid-state diffusion, infiltration, laser cladding, sol–gel coating combined with additive manufacturing, electrochemical synthesis, and high-energy ball milling. Recent studies indicate that core–shell architectures can offer enhanced control of reinforcement–matrix interactions by combining hard ceramic or carbide phases with more ductile metallic components. Rod-like Me@MeC/Fe (Me = Ta, Nb, W) architectures and dispersed core–shell particles show promising combinations of strength, toughness, and wear resistance, although their performance depends strongly on shell architecture, interface characteristics, and processing conditions. Remaining challenges include reproducible and scalable fabrication, shell architecture control, interface stability, and long-term performance. Further progress may benefit from advanced reinforcement design, additive manufacturing, modelling, and AI-assisted optimization of high-performance Fe-based MMCs.

Keywords: iron-based metal matrix composites (Fe-based MMCs); architectured reinforcements; core–shell structures; interface engineering; dispersion strengthening; powder metallurgy; additive manufacturing; mechanical properties

Check for updates

Academic Editor: Slobodan Mitrovic

Received: 9 August 2026
Revised: 2 September 2026
Accepted: 9 September 2026
Published: 10 September 2026

Copyright: © 2026 by the authors. Licensee MDPI, Basel, Switzerland. This article is an open access article distributed under the terms and conditions of the Creative Commons Attribution (CC BY) license.

1. Introduction

Iron and its alloys remain indispensable engineering materials owing to their low cost, well-established processing technologies, and broad range of mechanical properties. Their extensive application in automotive, energy, aerospace, chemical, and heavy industries is associated with a favorable combination of strength, toughness, manufacturability, and

economic efficiency. However, the increasing demands of advanced engineering systems require materials capable of operating under more severe conditions, including elevated temperatures, aggressive environments, severe wear, and extended service life. These challenges have stimulated continuous efforts to improve the performance of iron-based alloys through advanced microstructural design and composite reinforcement strategies [1–3].

Among various approaches developed to overcome these limitations, iron-based metal matrix composites (Fe-based MMCs) reinforced with dispersed strengthening phases have attracted considerable attention due to their ability to combine the toughness and processability of iron matrices with the high hardness, thermal stability, and wear resistance of ceramic or intermetallic reinforcements. Recent studies and reviews have demonstrated that Fe-based MMCs represent promising material systems for demanding applications where improved mechanical performance and service reliability are required. In particular, oxide-dispersion-strengthened steels and carbide-reinforced Fe-based composites have shown significant potential for applications involving high-temperature exposure, severe mechanical loading, and aggressive service environments [4–6].

The mechanical performance of Fe-based MMCs is governed not only by the intrinsic properties of the matrix and reinforcement phases but also by reinforcement size, morphology, spatial distribution, volume fraction, and, critically, the characteristics of the reinforcement–matrix interface. In conventional composites, particle agglomeration, insufficient wettability, undesirable interfacial reactions, and residual thermal stresses frequently limit strengthening efficiency and may lead to premature failure. Therefore, effective design of Fe-based MMCs requires simultaneous optimization of fabrication processes, reinforcement characteristics, and interfacial structure [7–9].

Various processing routes have been developed for manufacturing Fe-based MMCs, including powder metallurgy, mechanical alloying, hot consolidation, casting, infiltration, and additive manufacturing. Powder metallurgy approaches provide excellent possibilities for controlling reinforcement distribution and achieving homogeneous microstructures, whereas casting and infiltration methods offer advantages for large-scale production. More recently, additive manufacturing technologies have introduced new opportunities for producing complex reinforcement architectures and locally tailored microstructures. However, each processing route presents specific challenges related to densification, interface stability, reinforcement dispersion, and scalability [10–16]. A schematic comparison of the three principal fabrication routes for Fe-based MMCs and their typical industrial applications is presented in Figure 1.

Recent advances in reinforcement design have shifted research attention from simply increasing reinforcement content toward deliberate engineering of reinforcement morphology, spatial organization, and interfacial architecture. Unlike conventional approaches based mainly on increasing reinforcement fraction or reducing particle size, modern strategies increasingly focus on controlling reinforcement–matrix interactions through tailored interface design. In particular, architectured reinforcements, including core–shell structures, represent an emerging approach in which reinforcement architecture and interfacial characteristics are intentionally designed to achieve improved combinations of mechanical and functional properties.

Although numerous studies have investigated Fe-based MMCs, existing reviews have often focused on specific fabrication methods, reinforcement types, or individual strengthening mechanisms. A more integrated assessment of fabrication technologies, reinforcement architecture, interface characteristics, microstructural evolution, and resulting mechanical performance would therefore be valuable. This need is particularly relevant to architectured core–shell reinforcements, in which the shell introduces additional design variables, including composition, thickness, morphology, and interfacial characteristics,

that may influence load transfer, damage evolution, and the balance between strength, toughness, and durability.

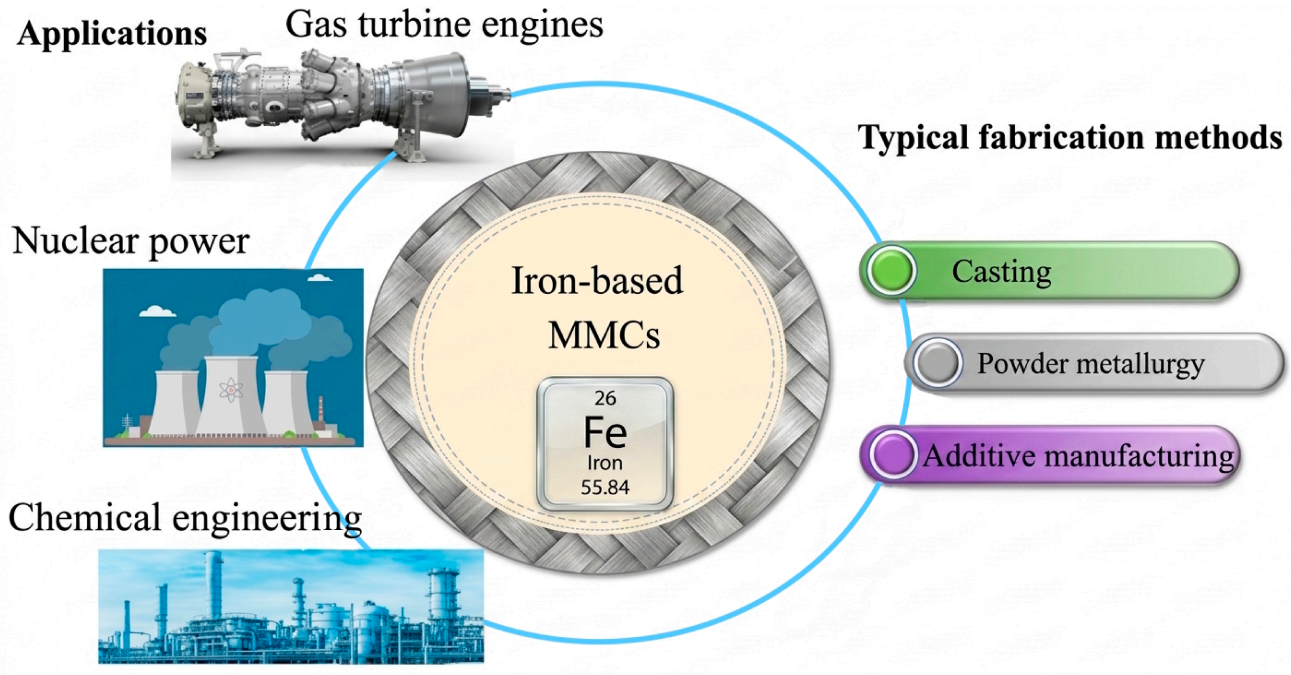


Figure 1. Schematic representation of the three major fabrication methods for Fe-based MMCs (powder metallurgy, casting, and additive manufacturing) and their primary industrial applications.

Against this background, the present review provides a comprehensive and critical assessment of recent developments in advanced Fe-based MMCs, with particular emphasis on architectured core–shell reinforcement systems. The review has three main objectives: (i) to compare powder metallurgy, casting, and additive manufacturing with respect to their processing characteristics, microstructural consequences, advantages, and limitations for Fe-based MMCs; (ii) to examine core–shell architectures by considering the effects of core/particle size, shell composition, shell thickness, morphology, and interface characteristics on load transfer, mechanical response, wear resistance, and interface stability; and (iii) to summarize the main limitations and research needs related to fatigue, corrosion, wear, high-temperature stability, scalability, and the development of more quantitative process–structure–property relationships. By bringing these aspects together, the review aims to provide an integrated perspective on how processing conditions, reinforcement architecture, and interface characteristics collectively influence the performance of Fe-based MMCs and to highlight directions for the further development of architectured reinforcement systems.

2. Methods for the Fabrication of Dispersion-Strengthened Iron-Based Metal Matrix Composites

The performance of iron-based metal matrix composites is governed primarily by the characteristics of the reinforcing phase, including its chemical stability, morphology, interfacial compatibility with the matrix, and resistance to degradation during both fabrication and service. An ideal reinforcement should maintain its structural integrity at elevated temperatures, exhibit good wettability and strong interfacial adhesion to the iron matrix, and avoid undesirable chemical reactions that may lead to the formation of brittle phases or degradation of mechanical properties.

A wide variety of ceramic reinforcements have been investigated for Fe-based MMCs, including refractory carbides (TiC, WC, SiC, and B_4C), borides (TiB_2), nitrides (Si_3N_4 and TiN), and oxides (Al_2O_3 and Y_2O_3) [7,8,17–20]. Their selection is primarily dictated by the requirement to preserve structural stability and mechanical integrity at temperatures exceeding 1000 °C during both processing and service [9]. Among these reinforcing phases, carbides—particularly TiC and WC—are the most widely employed because they combine high hardness with excellent wear resistance and relatively good thermophysical compatibility with iron matrices, thereby reducing residual thermal stresses generated during cooling [10,11]. In contrast, oxide particles such as Y_2O_3 are mainly used in oxide-dispersion-strengthened (ODS) steels, where their exceptional thermal stability effectively suppresses creep deformation and enhances high-temperature strength [5,6]. Nitride reinforcements, including Si_3N_4 and TiN, are generally considered for applications requiring superior chemical inertness and oxidation resistance under aggressive service conditions [12].

A schematic illustration of the principal reinforcement architectures used in Fe-based MMCs, including particulate, short-fiber, continuous-fiber, and layered reinforcements, is presented in Figure 2. Among these reinforcement geometries, particulate reinforcements remain the most widely adopted because of their relatively simple processing, good compatibility with powder metallurgy technologies, and ability to provide isotropic strengthening. Although continuous fibers and layered reinforcements offer more efficient load transfer and potentially higher mechanical performance, their application in iron-based systems remains limited owing to processing complexity, high manufacturing costs, and difficulties in achieving strong and thermally stable interfaces.

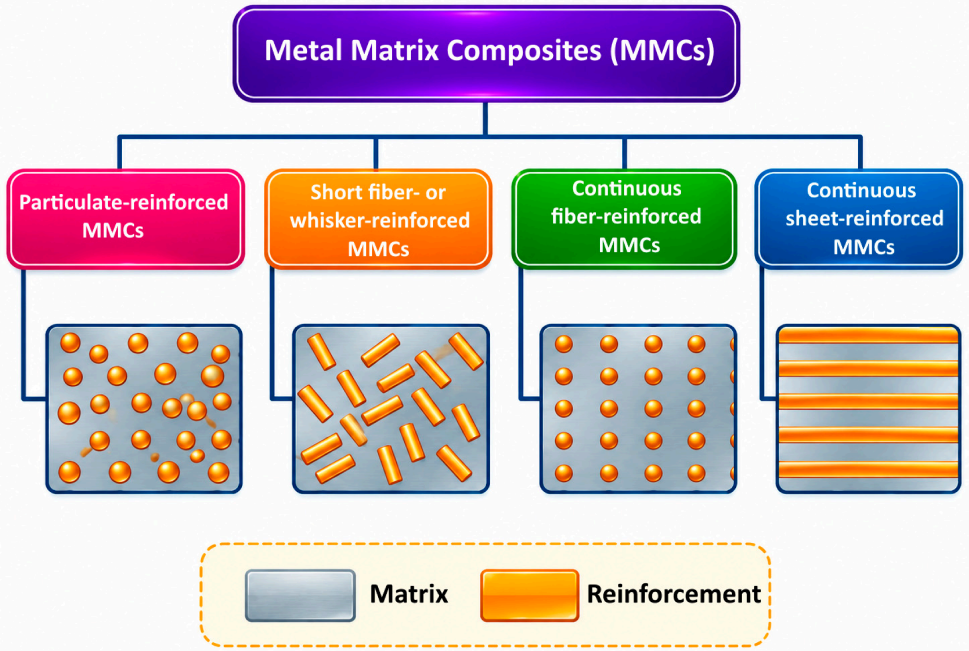


Figure 2. Reinforcement of iron-based metal matrix composites. Adapted from Ref. [15].

In addition to conventional ceramic reinforcements, considerable research efforts have recently focused on carbon nanomaterials, particularly carbon nanotubes (CNTs) and graphene [13]. Owing to their exceptional stiffness, tensile strength, and thermal conductivity, these nanostructures have attracted significant interest as potential reinforcing phases for Fe-based MMCs. Nevertheless, their practical implementation remains challenging because of severe particle agglomeration, limited wettability by iron, and the possibility of undesirable carbide formation during high-temperature processing, which may dete-

riorate the expected strengthening effect [13,14]. Consequently, ceramic reinforcements continue to dominate industrial applications owing to their superior processing stability, reproducibility, and technological maturity [2].

The selection of an appropriate reinforcing phase cannot be considered independently of the fabrication technology, since each processing route imposes specific requirements on particle size, morphology, surface chemistry, and thermodynamic stability. Therefore, understanding the advantages and limitations of different manufacturing methods is essential for the rational design of high-performance Fe-based MMCs. The most widely used fabrication routes include powder metallurgy, casting, and additive manufacturing, each offering distinct capabilities with respect to microstructural control, densification, production flexibility, and cost. These processing technologies are discussed in detail in the following sections.

2.1. Powder Metallurgy

Powder metallurgy (PM) remains the most widely employed and technologically mature route for the fabrication of dispersion-strengthened Fe-based MMCs because it provides excellent control over chemical composition, reinforcement content, and microstructural evolution [4,7,16,21]. Unlike conventional casting, PM enables the incorporation of thermodynamically stable ceramic particles without exposing them to prolonged contact with molten metal, thereby minimizing undesirable interfacial reactions and facilitating a more homogeneous distribution of the reinforcing phase. Consequently, powder metallurgy has become the benchmark processing technology for manufacturing Fe-based MMCs intended for high-temperature and wear-resistant applications.

The PM process generally consists of four principal stages: preparation of the powder mixture, compaction, sintering, and optional post-sintering thermomechanical processing [22]. Although each processing step appears straightforward, the final microstructure and mechanical performance of the composite are determined by the cumulative effect of these individual stages, making careful process optimization essential.

The principal stages of the powder metallurgy process are schematically illustrated in Figure 3. As shown in the figure, the fabrication route comprises powder preparation and mixing, compaction, sintering, and, where required, subsequent thermomechanical processing. Each stage plays a critical role in determining the final microstructure, interfacial characteristics, and mechanical performance of Fe-based MMCs. Consequently, careful optimization of every processing step is essential for achieving high-density composites with uniformly distributed reinforcing phases.

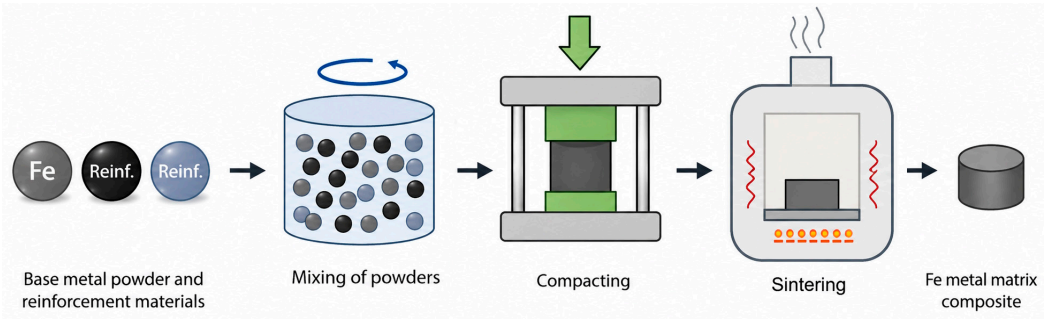


Figure 3. Schematic illustration of the powder metallurgy technique for preparing Fe MMCs.

2.1.1. Preparation of Powder Mixtures

The first stage involves homogeneous mixing of iron powders (or ferroalloy powders) with reinforcing particles. Mechanical blending using ball or planetary mills remains the most common approach because of its simplicity and scalability [4,23,24]. Alternatively,

chemical deposition techniques may be employed to achieve a more uniform distribution of reinforcement particles on the powder surface.

Achieving homogeneous dispersion is particularly challenging when nanoscale reinforcements are used. Their high specific surface area and strong van der Waals interactions promote severe particle agglomeration, resulting in heterogeneous microstructures and reduced strengthening efficiency. Various strategies have therefore been proposed to suppress agglomeration, including ultrasonic dispersion, the use of surfactants, and mechanical activation under carefully controlled milling conditions [25].

Another important challenge is the high affinity of iron powders for oxygen. Surface oxidation inhibits diffusion during sintering and weakens interfacial bonding between the matrix and reinforcing particles. Consequently, powder preparation is frequently performed under inert atmospheres such as argon or in reducing environments containing hydrogen, while pre-reduced powders are often employed to minimize oxygen contamination [26].

2.1.2. Powder Consolidation

Following powder preparation, the composite mixture is consolidated by cold pressing, hot pressing, or isostatic pressing [16,21]. Cold die pressing, typically performed at pressures between 400 and 800 MPa, produces green compacts with residual porosity that must subsequently be eliminated during sintering. In contrast, hot pressing combines mechanical pressure with elevated temperature (typically 900–1100 °C), promoting plastic deformation of powder particles, increasing densification, and significantly reducing pore volume. For components with complex geometries, cold or hot isostatic pressing provides more uniform pressure distribution, resulting in improved density homogeneity throughout the compact.

2.1.3. Sintering

Sintering is the most critical stage of powder metallurgy because it governs densification, diffusion bonding between matrix particles, and the formation of a mechanically robust reinforcement–matrix interface [27]. For Fe-based MMCs, sintering is generally conducted at temperatures ranging from 1100 to 1350 °C under carefully controlled atmospheres such as hydrogen, argon, vacuum, or mixed protective gases [14,28]. Hydrogen atmospheres are particularly advantageous because they effectively reduce surface oxides, thereby improving wettability, diffusion kinetics, and interfacial bonding.

The thermal stability of reinforcing particles is another key consideration during sintering. Ceramic phases such as TiC, WC, and SiC must retain their structural integrity without decomposing or reacting excessively with the iron matrix. Excessive interfacial reactions may result in the formation of brittle intermetallic compounds or eutectic structures, which deteriorate both strength and fracture toughness [28,29]. Therefore, optimization of the sintering temperature and holding time is essential to achieve an appropriate balance between densification and interfacial stability.

2.1.4. Hot Isostatic Pressing

Hot Isostatic Pressing (HIP) has become an important densification technique for advanced Fe-based MMCs, particularly those reinforced with ultrafine or nanoscale particles [16,21]. In HIP, simultaneous application of elevated temperature and isostatic gas pressure (typically 100–300 MPa) enables nearly complete elimination of residual porosity while promoting uniform diffusion throughout the material. Compared with conventional pressureless sintering, HIP generally produces composites with higher density, improved interfacial bonding, and superior mechanical properties.

Moreover, the enhanced densification achieved during HIP often permits lower processing temperatures or shorter holding times, thereby reducing grain coarsening and helping preserve the fine microstructure required for effective dispersion strengthening.

2.1.5. Post-Sintering Thermomechanical Processing

To further improve density and mechanical performance, sintered Fe-based MMCs are frequently subjected to thermomechanical processing, including hot extrusion or hot rolling [30]. These operations eliminate residual porosity, homogenize reinforcement distribution, refine the matrix microstructure, and improve particle–matrix bonding through intensive plastic deformation. Among these techniques, hot extrusion is particularly effective because it simultaneously increases density, enhances load transfer across the interface, and promotes the development of a refined microstructure, leading to superior strength and toughness.

Despite its numerous advantages, powder metallurgy still faces several important challenges. Oxidation of powder surfaces, agglomeration of nanoscale reinforcements, and insufficient interfacial bonding remain the principal factors limiting the full exploitation of dispersion strengthening in Fe-based MMCs. To overcome these issues, considerable research efforts have focused on oxygen-scavenging alloying additions (e.g., Ti, Zr, and Mg), protective coatings on reinforcing particles, and surface modification techniques such as nickel or copper deposition, all of which improve wettability and suppress oxidation during sintering [31].

Overall, powder metallurgy remains the benchmark fabrication route for dispersion-strengthened Fe-based MMCs because it provides exceptional flexibility in controlling reinforcement content, particle distribution, and microstructural evolution. Nevertheless, further progress depends on advances in powder surface engineering, oxidation control, nanoparticle dispersion, and interface design, which are expected to play a decisive role in the development of next-generation high-performance iron-based composites.

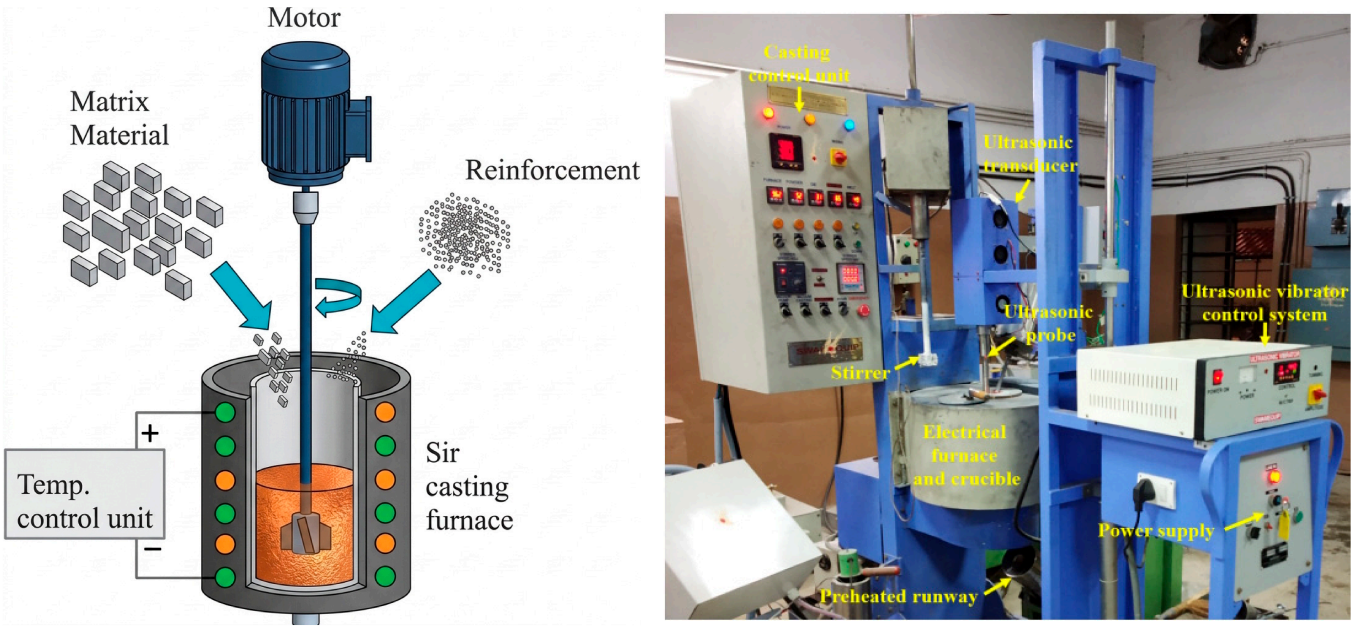
2.2. Casting Technologies

Casting represents one of the most productive and economically attractive routes for manufacturing MMCs. However, its application to Fe-based MMCs is considerably more challenging than to aluminum- or magnesium-based systems because of the high melting temperature of iron (1538 °C), the pronounced chemical reactivity of liquid iron, and the limited wettability of most ceramic reinforcements. Nevertheless, casting technologies continue to attract considerable interest, particularly for the production of large structural components and composites reinforced with micrometer-sized particles, for which powder metallurgy may become economically less favorable [32–34].

Among the available liquid-state processing routes, stir casting, squeeze casting, and melt infiltration are the three most widely investigated techniques for Fe-based MMCs. Although these methods differ in their processing principles, they all aim to achieve uniform reinforcement distribution while minimizing porosity, interfacial reactions, and segregation phenomena.

Stir casting is the simplest and most cost-effective technique, in which reinforcing particles are introduced directly into the molten metal and dispersed by mechanical or electromagnetic stirring [32]. A schematic representation of a typical stir-casting setup and a representative photograph of an ultrasonic-assisted stir–squeeze system are in Figure 4. As illustrated in the figure, successful processing requires simultaneous control of melt temperature, particle feeding, stirring intensity, and the processing atmosphere. The strong coupling between these parameters largely determines reinforcement dispersion and the quality of the reinforcement–matrix interface. Although the simplicity and scalability of

stir casting make it attractive for industrial applications, its use for iron melts is complicated by severe oxidation at elevated temperatures, insufficient wettability of ceramic particles, density-driven particle segregation, and accelerated wear of stirring equipment. Consequently, the process is generally performed under vacuum or in protective inert atmospheres (e.g., argon or helium) to suppress oxidation and stabilize melt behavior. The photograph (see Figure 4b) illustrates the general arrangement of the furnace/crucible, mechanical stirrer, ultrasonic probe, and pressure-assisted solidification unit. Although it originates from an Al-based composite study [35], it provides a representative view of the equipment configuration and processing sequence. For Fe-based MMCs, enhanced reinforcement dispersion, improved melt–particle contact, and pressure-assisted densification are particularly relevant. Recent studies using ultrasonic-assisted stir–squeeze processing [36,37] demonstrate the practical feasibility of combining intensive melt mixing with pressure-assisted solidification, providing a conceptual basis for developing analogous processing routes for Fe-based MMCs.



(**a**) (**b**)

Figure 4. Stir-casting apparatus: (**a**) schematic representation of the processing principle; (**b**) real ultrasonic-assisted melt-stirring/squeeze-casting setup. The photographic setup illustrates the furnace/crucible, mechanical stirrer, ultrasonic transducer and probe, control unit, power supply, and preheated runway. Reprinted from Ref. [37].

Squeeze casting overcomes several limitations of conventional stir casting by applying external pressure (typically 100–150 MPa) during solidification, thereby improving melt infiltration into the reinforcing phase and significantly reducing shrinkage porosity [33,34]. Pressure-assisted infiltration is particularly advantageous for ceramic reinforcements exhibiting poor wettability by liquid iron because it enhances interfacial contact and promotes more complete densification. As a result, squeeze casting enables the fabrication of composites containing relatively high reinforcement fractions (up to 30–40 vol.%) while maintaining low residual porosity. However, the requirement for specialized high-pressure equipment and carefully designed molds limits its application to specific component geometries.

Melt infiltration represents an alternative approach in which molten iron penetrates a porous reinforcement preform through capillary action, externally applied pressure, or a combination of both. Unlike conventional particle dispersion in the melt, this technique enables the fabrication of composites containing continuous or interconnected reinforcement

architectures, making it particularly attractive for wear-resistant and high-temperature applications. Refractory carbide preforms based on TiC or WC are among the most common systems processed by this route [38–40].

From a processing perspective, these casting routes differ primarily in the mechanism by which the reinforcing phase is incorporated into the matrix. Stir casting relies on mechanical particle dispersion, squeeze casting enhances reinforcement infiltration through applied pressure, whereas melt infiltration enables the fabrication of continuous reinforcement networks. Consequently, the selection of a casting route should be based not only on production cost and component geometry but also on the desired reinforcement architecture and interface characteristics.

Despite these technological differences, all liquid-state fabrication routes share several common scientific challenges associated with interfacial reactions, wettability, oxidation, particle segregation, and defect formation. These phenomena are strongly interconnected and ultimately determine the microstructure and mechanical performance of cast Fe-based MMCs.

2.2.1. Interfacial Reactions and Chemical Stability

One of the most critical limitations of casting Fe-based MMCs is the chemical interaction between molten iron and ceramic reinforcements. At elevated temperatures, liquid iron may partially dissolve or react with reinforcing particles, leading to the formation of brittle reaction products that deteriorate mechanical performance. Silicon carbide is a representative example, as its interaction with molten iron may result in the formation of iron silicides and carbon-containing reaction products, thereby reducing the expected strengthening effect. Consequently, thermodynamic compatibility between the reinforcement and the iron melt should be considered one of the primary criteria when selecting ceramic particles for casting-based Fe-based MMCs. Chemically stable carbides (TiC, WC) and oxides (Al_2O_3) are therefore generally preferred, although even these materials require careful control of processing temperature and melt contact time.

2.2.2. Wettability and Interfacial Bonding

Poor wettability of ceramic particles by liquid iron remains another major obstacle to the fabrication of high-quality cast composites. Insufficient wetting inhibits complete infiltration of the reinforcement and promotes the formation of interfacial voids, reducing the efficiency of load transfer between the matrix and the reinforcing phase. This issue has become one of the central topics of interface engineering in metal matrix composites over the past decade, and numerous studies have focused on improving the physicochemical compatibility between ceramic reinforcements and Fe-based melts.

2.2.3. Oxidation

Oxidation further complicates liquid-state processing. Exposure of molten iron to atmospheric oxygen results in the formation of oxide films and non-metallic inclusions that impair melt fluidity, reduce wettability, and increase the likelihood of pore formation. Oxidation not only degrades melt quality but also modifies interfacial chemistry, thereby affecting the nucleation and growth of reaction products during solidification. Consequently, industrial casting of Fe-based MMCs is generally performed under vacuum or protective inert atmospheres to maintain melt cleanliness and ensure reproducible processing conditions.

2.2.4. Particle Segregation and Agglomeration

Maintaining a homogeneous reinforcement distribution remains another major challenge. Density differences between the reinforcing phase and the molten matrix may lead

to either sedimentation or flotation of particles, while melt convection and solidification dynamics further influence their redistribution. For nanoscale reinforcements, this problem is compounded by strong particle agglomeration caused by their high surface energy. Therefore, reinforcement distribution depends not only on particle density but also on particle size, melt viscosity, stirring conditions, and solidification rate.

2.2.5. Porosity and Non-Metallic Inclusions

Porosity and oxide inclusions are common casting defects that significantly reduce ductility and fatigue resistance. Gas entrapment during stirring, insufficient melt degassing, and oxide formation all contribute to defect generation. These defects become particularly detrimental in nanocomposites because the large interfacial area increases the sensitivity of the composite to local stress concentrations.

To overcome these limitations, considerable research efforts have focused on improving both reinforcement design and processing conditions. Surface modification of ceramic particles through metallic coatings (Ni, Cu, Co, or Fe) has proven particularly effective because such coatings improve wettability, enhance interfacial bonding, and act as diffusion barriers that suppress undesirable chemical reactions between the reinforcement and molten iron. In this respect, coated particles represent an important intermediate step toward the architectured core–shell reinforcements discussed in later sections of this review.

Modification of the matrix composition provides another strategy for improving casting performance. Alloying additions such as Si, Mn, Cr, and Ni alter the physicochemical characteristics of Fe-based melts and may improve reinforcement wettability while simultaneously influencing reaction kinetics. In parallel, vacuum melting, induction melting under controlled atmospheres, and ultrasonic melt treatment have been successfully employed to reduce oxidation, promote particle dispersion, improve melt cleanliness, and suppress porosity. Finally, optimization of processing temperature and melt holding time remains essential for minimizing reinforcement degradation while ensuring sufficient melt fluidity for complete mold filling.

Although each of these strategies addresses a specific processing challenge, their combined implementation generally provides the greatest improvement in composite quality. Consequently, modern casting technologies increasingly rely on integrated process optimization rather than isolated modification of individual processing parameters.

Overall, casting remains a highly attractive manufacturing route for Fe-based MMCs because of its high productivity, scalability, and relatively low production cost, particularly for composites reinforced with micrometer-sized ceramic particles [32–34,38–40]. However, successful implementation requires simultaneous control of reinforcement wettability, interfacial reactions, oxidation, segregation, and defect formation. Recent advances in particle surface engineering, ultrasonic melt processing, controlled-atmosphere casting, and pressure-assisted infiltration are progressively expanding the capabilities of liquid-state processing and are expected to facilitate the production of increasingly sophisticated Fe-based composite architectures.

2.3. Additive Manufacturing

Additive manufacturing (AM) has emerged as one of the most promising technologies for the fabrication of metal matrix composites because it enables the production of components with complex geometries, tailored internal architectures, and localized compositional control that are difficult or impossible to achieve using conventional manufacturing methods. Unlike powder metallurgy and casting, AM builds components layer by layer directly from three-dimensional digital models, providing unprecedented flexibility in both structural design and material distribution. For Fe-based MMCs, this capability is

particularly attractive because it allows for precise control of reinforcement distribution while minimizing material waste and reducing the need for extensive post-processing.

Among the numerous AM technologies available for metallic materials, laser powder bed fusion (LPBF, also referred to as selective laser melting, SLM), directed energy deposition (DED), and electron beam melting (EBM) are the most extensively investigated for Fe-based MMCs [41,42]. Although these technologies differ in their energy source, powder delivery system, and deposition strategy, they share the common objective of producing dense metallic components through rapid localized melting and solidification. A schematic representation of a typical LPBF/SLM system is presented in Figure 5 [43].

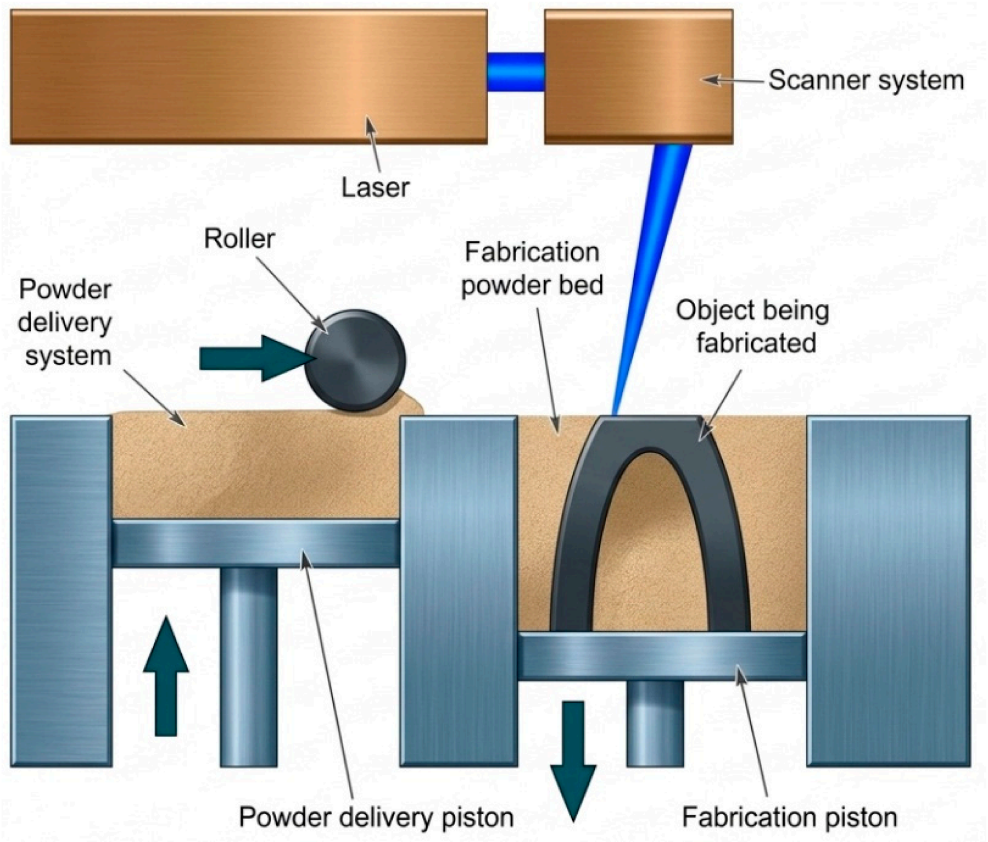


Figure 5. Schematic of a typical LPBF/SLM process setup. Adapted from Ref. [43].

2.3.1. Laser Powder Bed Fusion (LPBF/SLM)

Laser powder bed fusion is currently the most widely investigated additive manufacturing technique for Fe-based MMCs because it provides high dimensional accuracy and microstructural control. For MMC fabrication, the reinforcement can be introduced ex situ by premixing or mechanically alloying ceramic particles with the metal powder, by preparing a composite powder feedstock, or, in some powder-bed systems, by supplying a separate reinforcement fraction to the powder bed through the recoating sequence. Ex situ addition provides direct control over reinforcement chemistry and nominal fraction, but particle segregation, agglomeration, altered powder flowability, and incomplete wetting during melting may occur. In situ routes, in contrast, form the reinforcing phase during melting and solidification from reactive constituents; they can produce finer and more uniformly distributed phases and cleaner interfaces, but the final phase constitution depends strongly on local thermal history and reaction kinetics [44].

For iron-based alloys, LPBF/SLM typically employs gas-atomized spherical powders with particle sizes ranging from approximately 15 to 50 μm, ensuring good powder flowability and uniform layer deposition [41,42]. In MMC feedstocks, the addition of ceramic

particles changes packing density, flowability, laser absorption, thermal conductivity, and melt-pool behavior. Consequently, reinforcement fraction and particle size cannot be selected independently of laser power, scanning speed, hatch spacing, layer thickness, and preheating conditions. The mismatch in melting point and thermal expansion between Fe-based matrices and ceramic reinforcements may also promote incomplete wetting, interfacial reactions, residual stress, or cracking. These effects explain why feedstock preparation and process-parameter optimization must be treated as coupled variables in AM of MMCs [44].

These characteristics are particularly beneficial for Fe-based MMCs reinforced with ceramic particles. Compared with conventional processing routes, LPBF/SLM reduces reinforcement segregation and enables a more homogeneous distribution of strengthening particles throughout the matrix. Recent studies have demonstrated that hybrid micro- and nanoscale SiC reinforcements significantly improve the tensile strength of iron-based composites, reaching approximately 764 MPa, whereas the incorporation of TiC nanoparticles promotes the formation of dense microstructures with uniformly dispersed reinforcing phases and a reduced population of processing defects [41,42].

2.3.2. Directed Energy Deposition (DED)

Directed Energy Deposition differs fundamentally from LPBF in that powder or wire feedstock is delivered directly into a localized melt pool generated by a focused energy source. For MMCs, reinforcement can be introduced by premixing ceramic particles with the metallic powder feedstock, by feeding a pre-alloyed/composite powder, or by delivering the reinforcement through a separate powder-delivery channel or second nozzle. The latter configuration permits independent control of matrix and reinforcement feed rates and therefore facilitates spatial variation in reinforcement content and the fabrication of functionally graded structures. However, particle trajectories, capture efficiency, melt-pool residence time, wetting, and reaction kinetics must be controlled to avoid segregation and excessive interfacial reactions [44,45].

The localized nature of the melt pool provides flexibility in material composition and makes DED particularly attractive for MMC coatings, repair, large components, and compositionally graded materials. In multi-material DED, however, abrupt changes in composition can generate thermal-expansion and elastic/plastic-property mismatches, residual stresses, dilution, and local phase changes. Gradual variation in the matrix/reinforcement ratio can reduce these discontinuities and is one of the principal advantages of functionally graded materials (FGM) fabrication by powder-fed DED. At the same time, stable powder feeding and accurate control of the local composition remain challenging, especially when ceramic particles have substantially different density, morphology, or thermal properties from the metal powder [45].

2.3.3. Electron Beam Melting (EBM)

EBM, also termed electron beam powder bed fusion (EB-PBF), employs a focused electron beam as the heat source and is generally performed under vacuum, thereby minimizing oxidation during processing. The powder bed is typically maintained at an elevated temperature during fabrication, which reduces thermal gradients and residual stresses compared with many laser-based processes. These characteristics are advantageous for Fe-based MMCs containing brittle ceramic reinforcements, where rapid thermal cycling can promote cracking and interfacial damage [46].

For Fe-based MMCs, reinforcement can be introduced into EBM feedstock either by ex situ blending of matrix and reinforcement powders or by using pre-alloyed/composite powders in which the reinforcement is formed in situ before or during powder production.

The latter strategy is particularly attractive because spherical composite particles can provide better powder flowability and a more homogeneous reinforcement distribution than mechanically mixed powders. For example, gas-atomized Fe–TiC composite powder with TiC formed in situ was successfully processed by EB-PBF, producing more than 99% dense material with homogeneously distributed submicron TiC precipitates [46]. EBM can also be combined with alternative feedstock configurations; recent work demonstrated the fabrication of TiC/steel composites by combining EB-PBF with in situ liquid-metal infiltration, indicating that the high-temperature processing environment can be exploited to obtain dense composites with high ceramic contents [47].

An important consideration in EBM of MMCs is the interaction between the electron beam, metallic matrix, and non-melting reinforcement particles. Differences in melting point, electrical conductivity, thermal conductivity, density, and wettability can modify melt-pool flow and particle redistribution, making beam power, scan strategy, layer thickness, and preheating conditions important for controlling particle dispersion and defect formation. Experimental and modelling studies of EBM MMCs show that interfacial wetting and particle-induced changes in melt-pool flow can influence reinforcement agglomeration, while appropriate layer-wise processing can promote a more uniform distribution in the consolidated material [48]. Thus, the main advantages of EBM for Fe-based MMCs—vacuum processing, elevated build temperature, and reduced thermal gradients—must be considered together with the requirements for suitable composite powder flowability, electrical response, reinforcement distribution, and stable matrix–particle interfaces.

2.3.4. Binder Jetting for Fe-Based MMCs

Binder jetting (BJ) provides an additional AM route for MMCs in which a liquid binder selectively joins powder particles at room temperature, followed by depowdering, debinding, and sintering. For MMCs, metallic and ceramic powders can be blended before printing, and reinforcement distribution is therefore largely established in the feedstock rather than by a melt pool. This avoids beam-induced melting of the ceramic phase and can reduce thermally driven interfacial reactions during shaping. Nevertheless, BJ introduces its own challenges, including powder segregation, binder infiltration, dimensional shrinkage during sintering, residual porosity, and the need to select a sintering cycle that provides sufficient densification without undesirable reactions between the matrix and reinforcement [49].

2.3.5. Functionally Graded Materials in AM of Fe-Based MMCs

Additive manufacturing enables functionally graded MMCs by changing reinforcement content, matrix composition, or both along the build direction or within selected regions. In powder-fed DED, this can be achieved by independently metering two or more powder streams and continuously varying their feed rates; in PBF, graded structures can be produced by changing the composition of the powder layer between build regions or by using multiple feedstock strategies. The main advantage is the ability to place high reinforcement fractions where wear, stiffness, or thermal resistance is required while retaining a more ductile matrix elsewhere, thereby reducing abrupt property transitions. The principal challenges are compositional accuracy, powder mixing and delivery stability, dilution between successive layers, residual stresses caused by gradients in thermal and mechanical properties, and reproducibility of the local reinforcement fraction [45,50].

2.3.6. Post-Processing of AM Fe-Based MMCs

Post-processing is an important part of the AM route for Fe-based MMCs because the as-built state may contain residual porosity, residual stresses, rough surfaces, compositional heterogeneity, and metastable microstructures. Stress-relief annealing or other heat

treatments can reduce residual stresses and modify the matrix microstructure, whereas HIP combines elevated temperature and isostatic pressure to close internal pores, improve densification, homogenize the microstructure, and strengthen metallurgical bonding. For MMCs, the HIP or heat-treatment schedule must additionally account for reinforcement stability, possible interfacial reactions, and differences in thermal expansion and diffusion kinetics between the matrix and reinforcement. Machining, grinding, or surface finishing may subsequently be required where dimensional accuracy or surface integrity is critical [51].

EBM has been successfully employed to fabricate Fe–TiC and Fe–WC(Ni) composites exhibiting relatively uniform reinforcement distribution and satisfactory densification [41,42]. However, compared with LPBF, the broader melt pool and lower cooling rates may reduce the degree of microstructural refinement, while the high cost of equipment continues to limit widespread industrial implementation.

2.3.7. Current Challenges and Future Perspectives

Despite their significant advantages, additive manufacturing technologies still face several challenges that limit their broader application to Fe-based MMCs. Porosity remains one of the most common defects and generally originates from incomplete melting, unstable melt-pool dynamics, or inappropriate scanning parameters. Cracking is another critical issue arising from steep thermal gradients, rapid solidification, and the mismatch in thermal expansion coefficients between the metallic matrix and ceramic reinforcements. Oxidation of powders and molten material may further deteriorate interfacial bonding and increase defect formation if processing atmospheres are not carefully controlled.

Considerable research efforts have therefore focused on improving both feedstock design and process optimization. Protective metallic or ceramic coatings deposited on reinforcing particles enhance wettability and reduce undesirable interfacial reactions. In situ formation of reinforcing phases during printing offers an alternative strategy for achieving finer particle distributions and cleaner interfaces than conventional ex situ particle addition. Simultaneously, optimization of laser power, scanning speed, hatch spacing, and layer thickness, together with remelting strategies, has proven effective in reducing porosity, improving densification, and enhancing microstructural homogeneity.

Overall, additive manufacturing represents a high-flexibility processing route for Fe-based MMCs because it combines geometric freedom with precise control of microstructural evolution and reinforcement distribution. Nevertheless, successful implementation requires careful optimization of processing parameters, powder characteristics, and interfacial engineering to fully exploit the advantages of rapid solidification while minimizing defect formation.

2.4. Comparative Assessment of Fabrication Methods

The comparison in Table 1 highlights distinct processing windows and application-specific advantages among powder metallurgy, casting, and additive manufacturing. Representative quantitative values illustrate these differences: Fe powder compaction commonly employs pressures of about 400–850 MPa [2,7,14,16], while squeeze casting is typically conducted at approximately 100–150 MPa [32,33,38–40]. For Fe-based LPBF, representative processing conditions include laser powers of about 100–400 W, scan speeds of approximately 100–1300 mm/s, and layer thicknesses of about 30–80 μm [41–44]. Optimized Fe-based LPBF can achieve relative densities of approximately 99.45% [41–44]. These values should be regarded as representative processing windows rather than universal limits, since the optimum conditions depend on alloy chemistry, reinforcement fraction, powder characteristics, machine configuration, and component geometry.

Table 1. Comparison of fabrication methods for Fe-based metal matrix composites: processing characteristics, advantages, limitations, and industrial applicability.

Fabrication Method	Sub-Method	Feedstock/ Reinforcement Size *	Pressure/Energy Input *	Thermal/Layer Window *	Quantitative Indicator *	Principal Limitations	Representative Applications	Ref.
Powder metallurgy	-	Fe powder ~20–100 µm; reinforcement nano–micro	Compaction: 400–850 MPa; HIP: 100–300 MPa	Sintering ~850–1350 °C	Green density ~86–93%	Multistage processing; residual porosity; powder oxidation/agglomeration; tooling constraints	Wear-resistant components; structural MMCs; complex powder-based parts	[2,7,10,14,16,23,29]
Casting technologies	-	Primarily ~1–100 µm; nanoscale additions require dispersion aids	Squeeze pressure: 100–150 MPa	Fe melt ~1550–1650 °C	Near-net-shape capability	Poor wettability; segregation; porosity; reinforcement agglomeration; high melt temperature	Large components; near-net-shape structural and wear-resistant parts	[32,33,38–40]
Additive manufacturing	LPBF/SLM	Powder ~15–50 µm	Laser power ~100–400 W; scan speed ~100–1300 mm/s	Layer thickness ~30–80 µm	Relative density up to ~99.45%	High parameter sensitivity; residual stress; porosity; limited build volume; high equipment cost	Complex/high-precision components; tooling; aerospace; biomedical	[41–44]
	DED	Powder- or wire-fed	Laser power ~0.55–3.3 kW	Localized melt pool; relatively large deposited layers	High deposition rate; compositional flexibility	Lower resolution; dilution; porosity; thermal gradients; machining often required	Large components; repair/ remanufacturing; coatings; functionally graded structures	[44,45]
	EBM	Powder bed; typically ~50–150 µm	Electron-beam power up to ~3 kW	Layer thickness ~50–200 µm; elevated build temperature	Relative density > 99% demonstrated for Fe–TiC MMC	Vacuum requirement; higher surface roughness; lower dimensional resolution; restricted material range; high equipment cost	Complex structural components; high-temperature applications; aerospace/biomedical	[46–48]

* Quantitative values in Table 1 are representative ranges compiled from the cited studies; they are not universal process limits and vary with alloy chemistry, reinforcement fraction, feedstock characteristics, equipment configuration, and component geometry.

Powder metallurgy is particularly advantageous when precise control of reinforcement distribution, powder composition, and microstructural evolution is required, especially for fine- and nanoscale reinforcements. Its main limitations are the multistage nature of processing, powder oxidation and agglomeration, residual porosity, and the constraints imposed by compaction tooling. Casting, including pressure-assisted routes such as squeeze casting, offers higher productivity and better suitability for larger components and near-net-shape manufacturing, but reinforcement wettability, segregation, porosity, and the relatively high melting temperature of Fe-based alloys can complicate processing.

Additive manufacturing, particularly LPBF, provides greater geometric freedom and additional opportunities for spatial control of reinforcement distribution and microstructure. The high cooling rates and localized energy input can enable refined microstructures and complex architectures; however, the process is sensitive to powder characteristics and processing parameters, while residual stresses, porosity, cracking, reinforcement agglomeration, and high equipment costs remain important limitations.

Thus, the selection of a fabrication route should be based not on a universally superior process but on the required combination of reinforcement scale and distribution, component geometry, production volume, dimensional complexity, and targeted performance. Overall, the fabrication method determines not only the final shape of Fe-based MMC components but also the evolution of matrix microstructure, reinforcement distribution, and interfacial characteristics. Therefore, further development of high-performance Fe-based MMCs will require an integrated approach combining optimized processing routes with deliberate reinforcement architecture design. In particular, core–shell particles and other architectured reinforcements provide promising pathways for addressing some limitations of conventional dispersion strengthening by enabling greater control over particle stability, interface chemistry, and load-transfer mechanisms.

The following section discusses the relationship between microstructural characteristics and mechanical performance of Fe-based MMCs, focusing on the influence of grain refinement, reinforcement size, distribution, morphology, and interfacial characteristics on strengthening mechanisms and composite behavior.

3. Structure–Property Relationships in Fe-Based MMCs

As discussed in Section 2, the fabrication route selected for Fe-based MMCs (powder metallurgy, casting, or additive manufacturing) determines not only the macroscopic geometry of the component but also its microstructural characteristics, including matrix grain size, reinforcement distribution, particle morphology, and the nature of reinforcement–matrix interfaces. These structural parameters ultimately govern the mechanical response of the composite. Consequently, understanding the relationships among particle size, volume fraction, morphology, interfacial characteristics, and mechanical performance is essential for the rational design of high-performance Fe-based MMCs.

The mechanical behavior of Fe-based MMCs is controlled by a complex combination of strengthening mechanisms that operate simultaneously and frequently interact with one another. The most influential structural parameters include matrix grain size, dislocation density, reinforcement volume fraction, particle size and morphology, spatial distribution of reinforcing particles, and the quality of the reinforcement–matrix interface. Unlike conventional steels, where strengthening is achieved primarily through alloying and heat treatment, dispersion-strengthened MMCs rely heavily on the deliberate introduction of reinforcing phases to modify microstructural evolution and dislocation behavior.

Among these structural parameters, the reinforcement–matrix interface plays a particularly important role because it determines load-transfer efficiency, deformation compatibility, and damage evolution during mechanical loading. Therefore, modern Fe-based MMC design increasingly focuses not only on selecting appropriate reinforcement phases but also on controlling their surface characteristics, spatial organization, and interfacial structure. As a result, micromechanical modeling and advanced characterization approaches have become important tools for separating and quantifying the contributions of individual strengthening mechanisms.

3.1. Grain Refinement and Hall–Petch Strengthening

Among the various strengthening mechanisms operating in Fe-based MMCs, grain boundary strengthening remains one of the most fundamental mechanisms for polycrystalline metallic matrices. Grain boundaries act as effective barriers to dislocation motion; therefore, decreasing the grain size increases the density of barriers and raises the stress required for plastic deformation. This relationship is classically described by the Hall–Petch equation:

$$\Delta\sigma_{\mathrm{HP}} = \frac{k_y}{\sqrt{d}}, \tag{1}$$

where $\Delta\sigma_{\mathrm{HP}}$ is the Hall–Petch strengthening contribution, k_y is the Hall–Petch coefficient, and d is the average grain diameter [52].

A reduction in grain size from 990 μm to 116 μm results in a substantial increase in the Hall–Petch contribution to yield strength, illustrating why grain refinement is one of the primary objectives in the development of dispersion-strengthened MMCs [53]. In composite systems, grain refinement is often promoted by reinforcing particles that inhibit grain growth during processing. This effect can be described by the Hall–Petch–Zener relationship:

$$\Delta\sigma_{\mathrm{HPZ}} = KG_m\sqrt{\frac{3b\cdot V_p}{4d_p}}, \tag{2}$$

where K is a material constant, G_m is the matrix shear modulus, b is the Burgers vector, V_p is the reinforcement volume fraction, and d_p is the average particle diameter.

The equation indicates that decreasing the reinforcement size and increasing its volume fraction generally enhance the strengthening effect. Experimental evidence supporting this behavior was reported by Liang et al. [53], who investigated the effect of TiB_2 addition on the microstructure refinement and mechanical properties of as-cast and reheated A517 steel. As shown in Figure 6, the addition of 0.1 wt.% TiB_2 significantly refined the equiaxed γ-grain structure: the average grain size decreased from 990 ± 183 μm for the untreated steel to 116 ± 35 μm, while the volume fraction of the equiaxed γ-grain region increased from 5% to 67% [53]. This refinement was attributed to the decomposition of TiB_2 at elevated temperatures into free Ti and B, followed by the formation of TiN particles through reaction with residual nitrogen in the liquid steel. These TiN particles then acted as heterogeneous nucleation sites for δ-ferrite, promoting the columnar-to-equiaxed transition and subsequent grain refinement of the γ-grains during solidification [53].

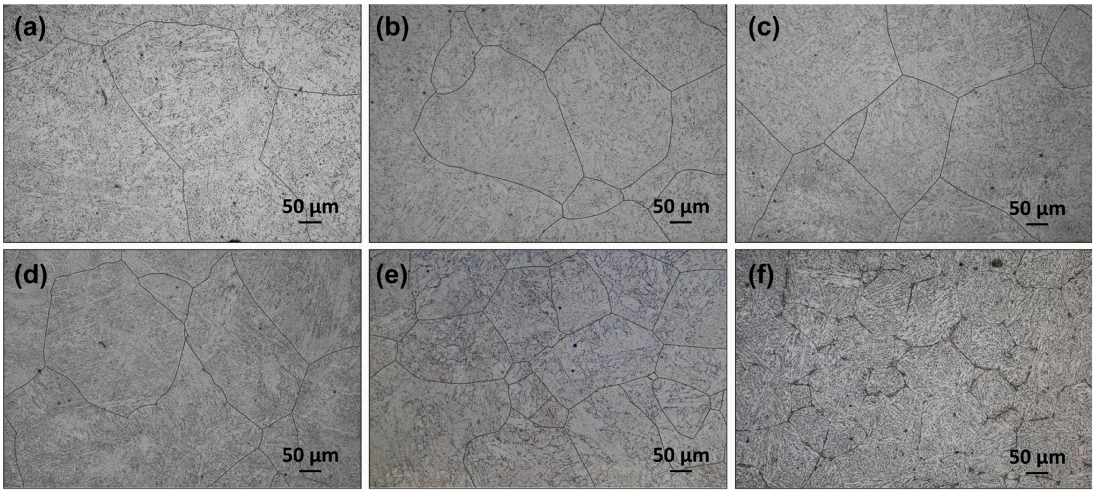


Figure 6. Optical micrographs of A517 steel after reheating at 1150 °C for 2 h with different TiB_2 additions: (**a**) 0, (**b**) 0.009, (**c**) 0.03, (**d**) 0.05, (**e**) 0.1, and (**f**) 0.5 wt.%. Reprinted from Ref. [53].

The tensile tests revealed a clear correlation between the microstructural changes and the resulting mechanical performance (see Figure 7). For the as-cast base steel (without TiB_2), the yield strength (YS), ultimate tensile strength (UTS), and elongation were 548 MPa, 700 MPa, and 15%, respectively; after reheating, these values improved to 620 MPa, 725 MPa, and 17%, reflecting a more uniform grain structure. Additions of 0.009, 0.03, and 0.05 wt.% TiB_2 produced only negligible changes in the tensile properties of the as-cast material, because the equiaxed-grain fraction remained below 50% and the gauge length still contained columnar grains. A marked enhancement was observed at 0.1 wt.% TiB_2, where the yield and tensile strengths rose to 599 MPa and 815 MPa—increases of 9.4% and 16.5% over the base values—while the elongation decreased slightly from 15% to 12%. This composition was regarded as optimal, providing the best compromise between strength and ductility. Further raising the TiB_2 content to 0.5 wt.% pushed the yield and tensile strengths to 609 MPa and 830 MPa, respectively, but severely damaged the ductility, with elongation dropping to only 6%. The strengthening at 0.1 wt.% TiB_2 is mainly attributable to grain refinement: the fine equiaxed grains (116 ± 35 µm) offer more grain boundaries that impede dislocation motion, in agreement with the Hall–Petch relationship (see Equation (1)). However, the concurrent precipitation of nanometre-sized Mo-rich borides along grain boundaries introduces crack initiation sites and reduces the elongation. At 0.5 wt.% TiB_2, these particles coarsen and even form eutectoid-type structures, promoting intergranular cracking and causing the dramatic loss of ductility. Overall, the mechanical behavior of TiB_2-modified A517 steel is governed by a competition between grain-refinement strengthening and precipitation-induced embrittlement.

Although grain refinement provides an effective strengthening contribution, its efficiency depends strongly on the ability of reinforcing particles to remain uniformly distributed and structurally stable during processing. This requirement highlights the importance of reinforcement architecture and interface stability in advanced Fe-based MMCs.

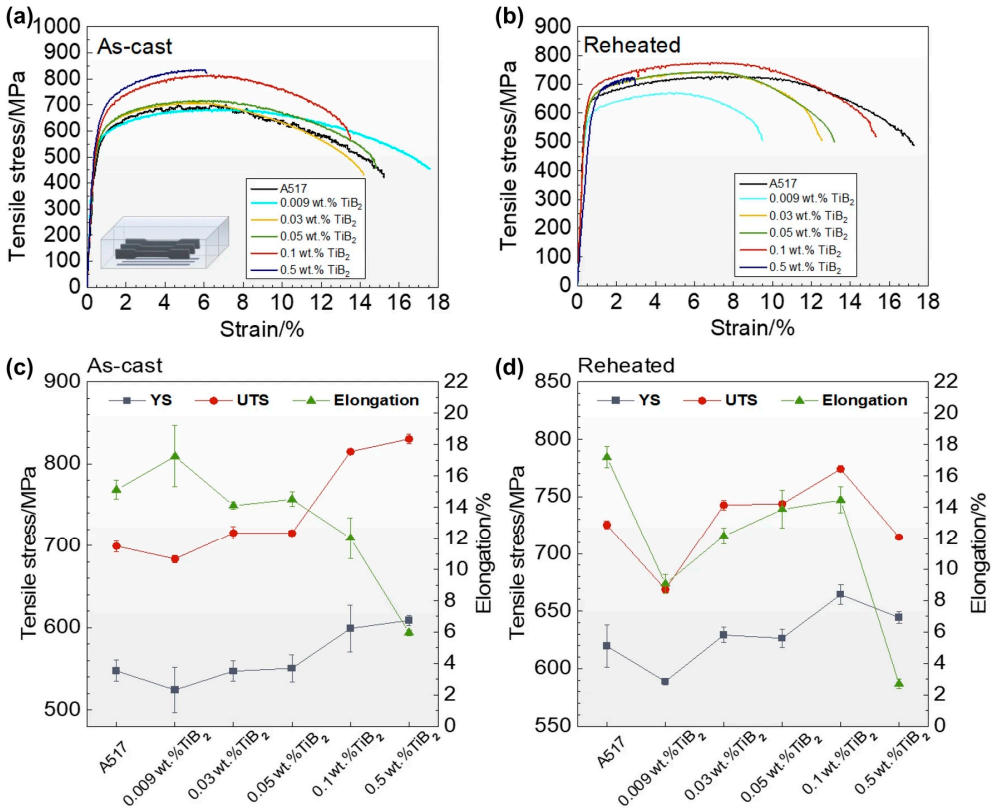


Figure 7. Effect of TiB_2 addition on the tensile properties of A517 steel: (**a**,**b**) typical engineering stress–strain curves for as-cast (**a**) and reheated (**b**) samples; (**c**,**d**) corresponding variations in yield strength (YS), ultimate tensile strength (UTS), and elongation with TiB_2 content for as-cast (**c**) and reheated (**d**) conditions. Reprinted from Ref. [53].

3.2. Limitations of Nanoscale Reinforcements

Although nanoscale reinforcing particles offer significant strengthening potential, their practical implementation is associated with several important technological and physical limitations. The first challenge is the synthesis of uniformly sized nanoparticles with narrow size distributions, which often requires sophisticated techniques such as laser ablation, plasma-assisted synthesis, or chemical vapor deposition, substantially increasing production costs.

A more critical issue is particle agglomeration. Because nanoparticles possess extremely high specific surface energy, they are thermodynamically unstable and tend to form clusters in order to reduce their surface energy. Such agglomerates behave as large defective inclusions rather than as effective nanoscale reinforcements. Consequently, they may fail to provide the expected strengthening effect and simultaneously act as stress concentrators that promote microcrack initiation and premature fracture.

In addition, non-uniform particle distribution creates reinforcement-depleted regions in which grain growth proceeds relatively unhindered, thereby reducing the effectiveness of Hall–Petch strengthening. These effects demonstrate that the transition from micro- to nanoscale reinforcement is not simply a matter of reducing particle size; successful implementation requires precise control of particle dispersion, interface stability, and processing conditions.

Consequently, current reinforcement strategies increasingly move beyond simple particle size reduction toward engineered reinforcement architectures, where surface modification and controlled interfaces are used to overcome the intrinsic limitations of nanoscale particles. Such approaches provide opportunities to improve particle stability, reduce agglomeration, and enhance compatibility with the Fe matrix.

3.3. Optimization of Reinforcement Content and Distribution

As noted in Sections 1 and 2, the reinforcing phases most commonly employed in Fe-based MMCs include refractory carbides (TiC, WC, SiC, and B_4C), borides (TiB_2), nitrides (Si_3N_4 and TiN), and oxides (Al_2O_3 and Y_2O_3) [7,8,54,55]. The optimization of composite microstructure therefore represents a multi-parameter problem in which grain refinement, particle size, reinforcement content, spatial distribution, and interfacial stability must be balanced simultaneously.

Modern approaches increasingly rely on high-energy mechanical alloying to achieve ultrafine grain structures and homogeneous particle dispersion, while spark plasma sintering (SPS) is employed to minimize grain coarsening during consolidation. However, recent studies have shown that excessive reinforcement contents may become detrimental. For example, reinforcement with more than approximately 4 wt.% nano-Al_2O_3 has been reported to cause significant embrittlement, rendering the material unsuitable for structural applications [56].

These observations demonstrate that simply increasing the amount of reinforcing phase is insufficient for achieving optimal performance. Instead, the strengthening efficiency depends on the interaction between reinforcement characteristics, matrix response, and interface behavior.

Consequently, current research is increasingly focused on integrated microstructural design strategies that combine controlled particle size, optimized reinforcement content, surface modification of reinforcing particles, hybrid reinforcement systems containing both micro- and nanoparticles, and carefully tailored processing conditions. Such approaches aim to maximize strengthening while preserving adequate ductility and fracture toughness.

However, achieving this balance remains challenging using conventional reinforcement strategies because the same particles responsible for strengthening may also introduce stress concentration sites and interfacial defects. This limitation has stimulated the development of architectured reinforcement concepts, where particle morphology and interface structure are designed as integrated elements of the composite architecture.

3.4. Implications for Advanced Reinforcement Architectures

The analysis presented above demonstrates that the mechanical performance of Fe-based MMCs is governed not only by the fabrication route but also by the size, distribution, morphology, and interfacial condition of the reinforcing particles. At the same time, the discussion highlights the fundamental limitations associated with conventional reinforcement strategies, particularly nanoparticle agglomeration, oxidation, insufficient wettability, and limited interfacial compatibility.

These limitations indicate that further improvements in Fe-based MMCs require not only finer particles or higher reinforcement fractions but also more sophisticated control of reinforcement architecture and interface design. In this context, surface-engineered particles and architectured core–shell reinforcement architectures have emerged as particularly promising approaches because they enable simultaneous control of particle stability, wettability, interfacial bonding, diffusion behavior, and deformation mechanisms.

Unlike conventional particles, core–shell reinforcements introduce an additional structural parameter through the deliberate design of the shell composition, thickness, morphology, and mechanical response. This approach provides new opportunities to combine hard strengthening phases with more compatible transition layers, thereby improving load-transfer efficiency while reducing detrimental interfacial stresses.

The following section therefore focuses on the fabrication methods, functional mechanisms, and design principles of architectured core–shell reinforcing particles, which provide a promising pathway for overcoming the limitations of conventional dispersion strengthening and for achieving an improved balance between strength, ductility, and long-term structural stability in Fe-based metal matrix composites.

4. Architectured Core–Shell Reinforcements for Fe-Based Metal Matrix Composites

4.1. Concept and Classification of Core–Shell Reinforcements

Core–shell reinforcement design treats the reinforcement and its interface as a single functional unit. The defining feature is a distinct core surrounded by a shell whose composition, thickness, morphology, and phase constitution are deliberately controlled (see Figure 8). This architecture adds an interfacial design variable to conventional particle reinforcement and allows the mechanical and chemical transition between the core and Fe matrix to be tailored [57–67].

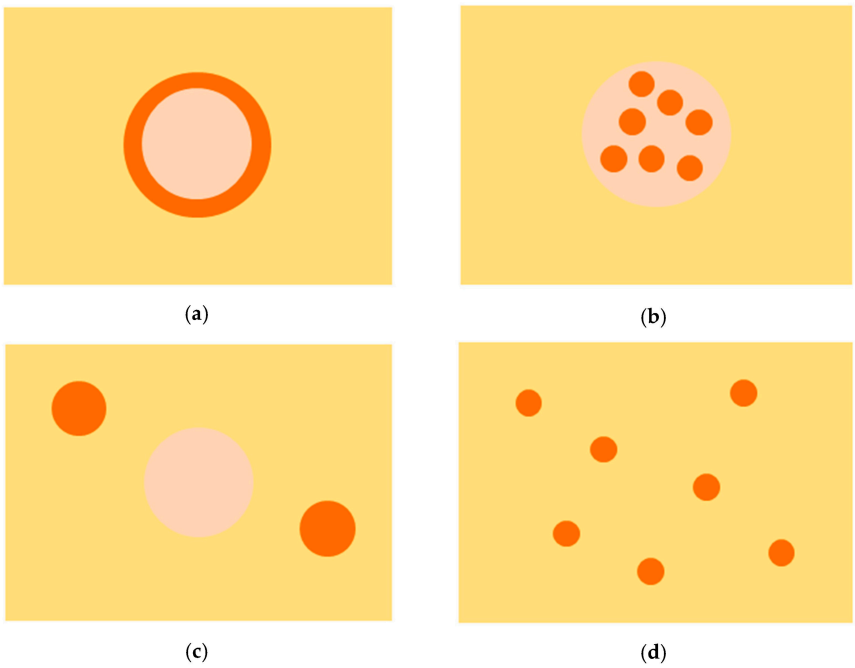


Figure 8. Possible microstructures of metal matrix composites. Yellow denotes the matrix, brown denotes the shell, and beige denotes the core: (**a**–**c**) two-phase composites with reinforcing particles of different shapes and spatial arrangements embedded in a matrix; (**d**) a composite containing only shell-material particles (no core material). Case (**a**) represents a core–shell particle-reinforced composite. The volume fraction of the core material is identical for cases (**a**–**c**), and the volume fraction of the shell material is the same for all cases (**a**–**d**). Reprinted from Ref. [61].

Conventional ceramic particles such as TiC, WC, SiC, TiB_2, Al_2O_3, and Y_2O_3 can provide high hardness, wear resistance, and high-temperature stability, but their performance may be limited by poor wetting, thermal-expansion mismatch, agglomeration, and interfacial reactions. Core–shell architectures address these limitations by introducing an intermediate phase that can improve compatibility with the Fe matrix while preserving the desired properties of the core [57–60].

The shell may serve several functions simultaneously: metallic shells can improve wettability and metallurgical bonding; carbide, nitride, or oxide shells can provide hardness, chemical stability, or diffusion control; and multilayer or graded shells can distribute stresses and regulate crack propagation. Thus, shell architecture should be selected together with the matrix and processing route rather than treated as a conventional protective coating [61,64–66,68–70].

Reported architectures range from coated or multilayer particles to in situ carbide shells, diffusion-controlled reaction layers, rod-like metal–carbide structures, fibers, and spatially organized reinforcement networks. The representative systems below are therefore grouped primarily by architecture and fabrication strategy, while their mechanical consequences are discussed separately in Section 4.3.

The key design principle is to integrate reinforcement chemistry, shell structure, and matrix compatibility. This distinction separates the architectural concept discussed here from simple particle coating and provides the basis for comparing the systems summarized in Table 2.

4.2. Representative Architectured Core–Shell Reinforcement Systems

Table 2 summarizes representative Fe-based MMCs containing core–shell or closely related architectured reinforcements. The systems are intentionally diverse in core chemistry, shell constitution, fabrication route, and geometry, allowing for comparison of how architecture is used to modify mechanical response.

Among the most extensively investigated systems are carbide-based core–shell reinforcements produced through in situ reactions and diffusion-controlled processes. The Nb–NbC/Fe core–shell rod composite represents a typical example, where a metallic Nb core is surrounded by a NbC-containing shell with a hierarchical laminated interface structure. The formation of this architectured reinforcement provides a stable metallurgical interface and a controlled transition between the reinforcement and Fe matrix [64]. Similar design principles have been demonstrated in W@WC/Fe composites, where a graded WC–Fe shell surrounding the W core creates a hierarchical reinforcement architecture combining a hard carbide region with a metallic core [65]. In addition, V_8C_7/Fe core–shell rod-reinforced composites demonstrate the potential of carbide-based architectures for developing stable reinforcement systems through diffusion-controlled carbide formation [66].

Beyond single-layer carbide shells, more complex metal–carbide architectures have been developed to achieve improved structural functionality. Ta–TaC/Fe composites provide an effective example in which a ductile Ta core is combined with a TaC-containing shell, forming an integrated metal–carbide reinforcement system [68,69]. Similarly, W–WC/Fe composite fibers extend the core–shell concept from rod-like reinforcement toward fiber-based architectures, providing additional opportunities for controlling reinforcement geometry and composite performance [70].

In addition to carbide-based systems, ceramic multilayer and coating-based architectures have recently attracted increasing attention. The Al_2O_3@TiC@TiB/Fe multilayer ceramic reinforcement demonstrates the application of hierarchical ceramic architectures for controlling microstructural development during laser cladding processes [71]. Furthermore, advanced manufacturing technologies have enabled the fabrication of new core–shell-based reinforcement systems, including WC–Co core–shell powders for laser cladding, TiO_2@WC/316L composites produced by selective laser melting, and WC-reinforced stainless-steel deposits fabricated by laser melting deposition [72–74]. These approaches expand the possibilities for designing spatially controlled reinforcement distributions and architectured interfaces.

Metallic shell-assisted reinforcement strategies represent another important development direction for Fe-based composite coatings. TiC–Ni-reinforced systems demonstrate the advantages of introducing metallic phases to improve ceramic–metal compatibility and facilitate the fabrication of wear-resistant Fe-based coatings [75,76].

Taken together, the examples show that core–shell reinforcement is not restricted to a single processing route or geometry. In situ diffusion and reaction routes are particularly effective for rod-like metal–carbide architectures, whereas coating, cladding, and AM routes provide additional control over particle-scale and spatially graded structures.

4.3. Strengthening Mechanisms of Architectured Core–Shell Reinforcements

The mechanical benefit of core–shell architectures can be understood through several coupled mechanisms: load transfer across a strong metallurgical interface, stress redistribution through graded or layered shells, HDI strengthening caused by mechanical contrast, grain refinement, and crack deflection or bridging. Their relative importance depends on shell thickness, phase constitution, interface continuity, and the deformation response of the core and matrix.

One of the primary advantages of core–shell architectures is the improvement of interfacial load transfer efficiency. In conventional MMCs, weak interfaces and insufficient wettability may lead to particle debonding and premature failure under external loading. In contrast, diffusion-generated carbide shells, such as NbC–Fe, TaC–Fe, and WC–Fe layers, establish strong metallurgical bonding with the Fe matrix and provide a gradual transition between the reinforcement core and surrounding matrix (see Figure 9). This interfacial design reduces stress concentration at the interface and enables more efficient transfer of external loads from the matrix to the reinforcing phase [64,68–70,77].

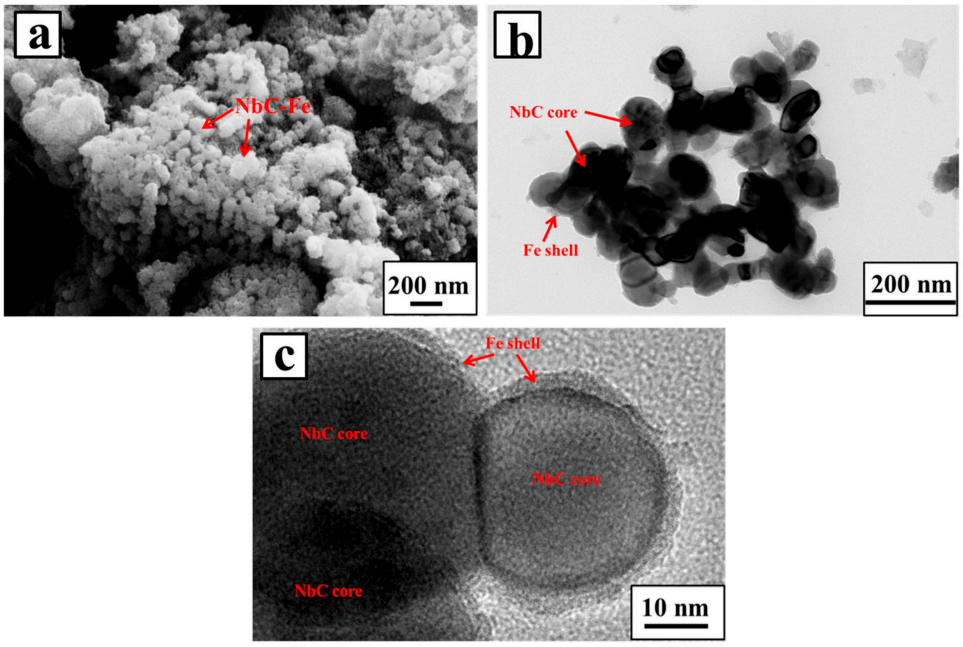


Figure 9. (**a**) SEM image, (**b**) TEM image, and (**c**) HRTEM image of the NbC-Fe nanocomposite powder obtained by electrochemical reduction of Nb_2O_5/Fe/carbon composite pellets at 900 °C under 3.0 V for 10 h. Reprinted from Ref. [77].

Table 2. Comparative characteristics of representative core–shell reinforcement architectures in Fe-based metal matrix composites.

Core–Shell Reinforcement Architecture	Matrix/Fabrication Method	Structural Characteristics	Particle Size/Shell Thickness	Mechanical Performance	Ref.
Nb–NbC/Fe core–shell rod	Cast-iron matrix; two-step in-situ reaction	Nb core with a two-zone NbC–Fe shell: inner NbC/α-Fe/NbC laminated region and outer dense NbC–Fe region	Nb rod: Ø1.5 × 14 mm; shell thickness not quantitatively reported	YS: 1623 MPa; UCS: 1970 MPa; FS: 11.3%; shell fracture toughness: 4.6 ± 0.2 and 4.0 ± 0.1 MPa·m$^{1/2}$	[64]
	Cast-iron matrix; two-step in-situ solid-phase diffusion	Metallic Nb core surrounded by NbC/Fe shell	Nb rod: Ø1.5 mm × 10 mm; shell thickness: 90 ± 3 to 233 ± 5 μm for 1–10 h soaking time	YS: 1794.4 MPa; FS: 11.6%; NbC/Fe shell hardness 12.86 GPa	[78]
W@WC/Fe core–shell bar	Iron matrix; infiltration + in-situ solid-phase diffusion + heat treatment	W core with graded WC–Fe shell and hierarchical interface architecture	W–WC/Fe composite fiber diameter ≈ 655 μm; W core ≈ 285 μm; calculated WC–Fe shell thickness ≈ 185 μm	YS: 2326 ± 23 MPa; UCS:3045 ± 19 MPa; FS: 23.6 ± 1.3%; wear resistance improved by 234.2 times compared with cast iron	[65]
	Iron matrix; casting + in-situ solid-phase diffusion at 1145 °C	Residual W core with gradient WC–Fe shell; W-core diameter decreases and shell thickness increases with diffusion time	No specific core diameter or shell thickness reported in the available article data	At 18 h: UCS 1100 ± 18 MPa; FS 35.5 ± 1.3%	[79]
V_8C_7/Fe core–shell rod	Iron-based matrix; two-step in-situ reaction at 1150 °C × 5 min + 1100 °C × (4–10 h)	Ductile metallic V core surrounded by a gradient-structured V_8C_7/Fe shell; shell contains V_2C, V_8C_7 and α-Fe phases. Increasing reaction time progressively increases shell thickness and decreases the V-core; *K* denotes the shell/core volume ratio	V rod: Ø1.75 × 12 mm; 4 h: shell 432 ± 12 μm, core 515 ± 9 μm, K = 5.2; 6 h: shell 643 ± 15 μm, core 382 ± 8 μm, K = 18.3; 8 h: shell 775 ± 18 μm, core 276 ± 8 μm, K = 54.0; 10 h: shell 896 ± 20 μm, core 225 ± 7 μm, K = 122.0	8 h: maximum hardness ~1296 $HV_{0.2}$, UCS: 1804 MPa, FS: 13.9%. UCS at 4, 6, and 10 h: 1445, 1630, and 2005 MPa, respectively; FS: 11.8%, 12.7%, and 12.3%, respectively. 8 h (K = 54) provides the best strength–toughness balance	[66]

Table 2. *Cont.*

Core–Shell Reinforcement Architecture	Matrix/Fabrication Method	Structural Characteristics	Particle Size/Shell Thickness	Mechanical Performance	Ref.
Metal–carbide/Fe core–shell structures (Ta–TaC, Nb–NbC, W–WC)	Iron matrix; in-situ solid-phase diffusion. Carbon diffuses from the Fe matrix into the surfaces of Ta, Nb and W rods, forming TaC, NbC and WC shells, respectively	Rod-shaped metallic Ta, Nb or W cores surrounded by corresponding TaC, NbC or WC carbide shells. Metallurgical integration is formed between the core–shell reinforcement and Fe matrix; carbide shells are produced directly by solid-state carbon diffusion	Pure-metal rods as cores: Ta (Ø2.0 mm, 99.99% purity), Nb (Ø1.5 mm, 99.99% purity), and W (Ø0.8 mm, 99.99% purity), surrounded by corresponding TaC, NbC, and WC carbide shells formed by in-situ carbon diffusion from the Fe matrix. The study compares Ta–TaC, Nb–NbC and W–WC architectures	Yield strength: 1981 MPa; ultimate compressive strength: 2238 MPa; fracture strain: 11.8%; fracture toughness: 5.89 (NbC–Fe shell) MPa·$m^{1/2}$; hardness: 1988 $HV_{0.05}$ (NbC–Fe shell), 1832 HV $HV_{0.05}$ (TaC–Fe shell),	[68]
Ta–TaC/Fe core–shell rod	Iron-based matrix; in-situ solid-phase diffusion reaction at 1150 °C for 5, 10, 15, 20, and 80 min	Metallic Ta core surrounded by a dense, compact gradient TaC–Fe shell. The shell consists of a TaC-rich layer with a gradient distribution toward the Fe matrix; predominant phases are Ta, TaC and α-Fe. TaC formation results from solid-state diffusion of C from the Fe matrix into the Ta rod	Initial Ta rod: 99.99% Ta (wt.%), diameter 2 mm; TaC–Fe shell thickness: 5 min: $(59.10 \pm 1.80) \times 10^{-4}$ cm; 10 min: $(95.40 \pm 5.51) \times 10^{-4}$ cm; 15 min: $(125.20 \pm 3.68) \times 10^{-4}$ cm; 20 min: $(152.30 \pm 6.37) \times 10^{-4}$ cm. Shell thickness increases progressively with annealing time	Impact toughness: 100.6 J·cm^{-2}; TaC–Fe shell hardness: 24.8 ± 0.53 GPa; elastic modulus: 506.6 ± 4.62 GPa	[69]

Table 2. *Cont.*

Core–Shell Reinforcement Architecture	Matrix/Fabrication Method	Structural Characteristics	Particle Size/Shell Thickness	Mechanical Performance	Ref.
W–WC/Fe composite fibers	Fe matrix; combination of infiltration and in-situ solid-phase diffusion, prepared at 1145 °C for 18 h	Aligned W–WC/Fe composite fibers embedded in an Fe matrix. Ductile W core surrounded by a gradient WC–Fe shell, with decreasing WC fraction and grain size toward the Fe matrix and increasing α-Fe fraction; strong interfacial bonding is achieved	Initial W fiber (99.99% W wt.%): Φ0.6 × 80 mm; after in-situ diffusion: W core diameter ≈ 287 μm, WC–Fe shell thickness ≈ 184 μm, giving a composite-fiber diameter of ≈ 655 μm.	YS: 701 ± 16 MPa; UCS: 1100 ± 18 MPa; FS: 35.5 ± 1.3%. For comparison, cast Fe: 365 ± 20 MPa YS, 834 ± 15 MPa UCS and 26.9 ± 1.1% FS. The architecture simultaneously improves strength and toughness through the synergistic effect of high-strength W–WC/Fe fibers and the tough Fe matrix	[70]
WC–Co core–shell powder/laser cladding layer	420 stainless steel matrix; high-energy ball milling to coat 420 powder with nano WC–Co, followed by laser cladding on 316L stainless-steel substrate	Spherical 420 stainless steel core particles uniformly coated with a nano WC–Co shell. The core–shell structure suppresses WC segregation during laser cladding and promotes a uniform distribution of nano WC–Co in the cladding layer; dense, crack- and pore-free cladding layers are obtained	420 stainless steel powder: D_{50} = 89.7 μm; nano WC–Co: 80–100 nm. WC–Co nanoparticles are uniformly distributed over the 420 particle surface	Microhardness of the cladding layer is significantly enhanced (up to ~500–600 HV) by the core–shell WC–Co reinforcement; the resulting cladding layer is dense and free of cracks and pores, with uniform nano WC–Co distribution and improved surface properties	[72]
Al_2O_3@TiC@TiB multilayer ceramic reinforcement	Fe-based coating; laser cladding on Q235 substrate using Fe60, 80TiFe and B_4C pre-alloyed powders; α-Al_2O_3 added as a nucleation substrate	α-Al_2O_3 core surrounded sequentially by TiC and TiB shells, formed in situ. α-Al_2O_3 promotes heterogeneous TiC nucleation, while TiC acts as a substrate for TiB growth; orientation relationships: Al_2O_3(104)//TiC(111) and TiC(111)//TiB(210)	Multilayer ceramic particles; no specific core diameter or shell thickness reported in the available article data	Grain size reduced by 16.2% and microhardness increased by 10.5% compared with the coating without α-Al_2O_3. The multilayer core–shell structure promotes grain refinement and enhanced hardness (up to ~880.3 $HV_{0.2}$)	[71]

Table 2. *Cont.*

Core–Shell Reinforcement Architecture	Matrix/Fabrication Method	Structural Characteristics	Particle Size/Shell Thickness	Mechanical Performance	Ref.
TiO_2@WC/316L composite	316L stainless-steel matrix; selective laser melting (SLM) using 4 wt% TiO_2@WC reinforcement	WC core particles uniformly coated with a TiO_2 shell by hydrolysis of a titanium precursor. The TiO_2 coating suppresses detrimental reactions between WC and the 316L matrix and promotes strong metallurgical bonding and homogeneous WC dispersion	WC particles: 10–53 μm; TiO_2 shell formed uniformly on the WC particle surface; no specific shell thickness reported	YS: 565 ± 5 MPa; UCS: 782 ± 5 MPa; plastic strain: 36.2%. Wear depth reduced by 36.8% under 60 N and 3 Hz compared with unreinforced 316L	[73]
NbC–Fe core–shell composite powder	Low-carbon steel matrix; electrochemical reduction and carbonization of Nb_2O_5/Fe/C precursor in molten $CaCl_2$–NaCl at 900 °C, followed by casting	NbC nanoparticles as cores surrounded by an Fe shell. The Fe shell provides strong interfacial bonding with NbC, improving wettability and sinterability and enabling a uniform distribution of carbide particles in steel	NbC cores: several nm; NbC–Fe composite particles: ~100 nm. The NbC nanoparticles are embedded/embraced by the Fe shell; specific shell thickness is not reported	Addition of 0.15 wt% NbC–Fe composite powder to low-carbon steel reduced the average cast-steel grain size from >1 mm to <500 μm and increased microhardness (up to 30 HV) compared with steel without NbC addition (19 HV)	[77]

The hierarchical shell structure further enhances mechanical performance by controlling crack initiation and propagation. The Nb–NbC/Fe system represents a typical example, where the shell consists of an inner NbC/α-Fe/NbC laminated region and an outer dense NbC–Fe layer. The laminated architecture improves fracture resistance by forcing cracks to deviate from their original propagation paths and increasing the energy required for crack propagation. Consequently, the Nb–NbC/Fe composite achieves a favorable combination of high strength and reasonable toughness compared with conventional cast iron [64].

A similar strengthening mechanism is observed in Ta–TaC/Fe composites, where a ductile Ta core is combined with a hard TaC-containing shell. The metallic core contributes to damage tolerance and accommodates deformation, whereas the carbide shell provides high hardness and wear resistance. The diffusion-generated interface ensures strong bonding between the reinforcement and matrix, preventing premature interfacial failure under impact loading conditions [68,69].

Another important strengthening mechanism is HDI strengthening. In W@WC/Fe composites, the large mechanical contrast between the hard WC-rich shell and ductile Fe matrix generates geometrically necessary dislocations during plastic deformation. These additional dislocations contribute to local strengthening while maintaining the deformation capability of the composite. Furthermore, the graded WC–Fe interface improves stress redistribution and contributes to the combination of high strength and wear resistance reported for these composites [65,70].

Microstructural refinement and heterogeneous nucleation provide additional strengthening contributions in multilayer ceramic core–shell systems. The Al_2O_3@TiC@TiB-reinforced Fe-based composite coating demonstrates that hierarchical ceramic architectures can promote heterogeneous nucleation during processing, resulting in refined microstructures and improved hardness. The multilayer ceramic structure contributes simultaneously to grain refinement, interface stabilization, and enhanced resistance to plastic deformation [71].

For oxide-containing shell architectures, strengthening is mainly associated with chemical stabilization and suppression of undesirable interfacial reactions. In TiO_2@WC/316L composites, the TiO_2 shell acts as a protective layer that limits direct interaction between WC reinforcement and the steel matrix. Maintaining reinforcement integrity contributes to improved mechanical balance between strength and ductility [73,74].

Metallic shell architectures provide another effective strategy for improving interfacial compatibility between ceramic reinforcements and metallic matrices. In TiC–Ni-reinforced coatings, the Ni-containing shell improves wettability between TiC particles and Fe-based substrates, enhances metallurgical bonding, and promotes more efficient stress transfer across the interface. These effects result in improved hardness and wear resistance of the deposited coatings [75,76].

Thus, the shell is a mechanically active region rather than only a barrier layer. Its principal contribution is to control how stresses and defects are transferred between the core and Fe matrix; this provides a unifying explanation for the strength–toughness combinations reported for several core–shell systems.

4.4. Effect of Shell Thickness and Shell Composition on Load Transfer and Damage Tolerance

Shell thickness directly controls the balance between reinforcement efficiency and damage tolerance. The Nb–NbC/Fe system provides one of the clearest quantitative examples: increasing the NbC–Fe shell from 90 ± 3 μm to 233 ± 5 μm with increasing diffusion time produced a pronounced change in mechanical response, while the composite processed for 7 h reached a maximum yield strength of 1794.4 MPa and a strain of 11.6% [78]. This demonstrates that shell growth is not merely a geometrical change; it changes the load-bearing fraction of the hard phase and the distance over which stresses are transferred from the matrix to the metallic core.

As shell thickness increases, the hard carbide fraction and the effective load-bearing cross-section generally increase, which can raise strength and hardness. However, an excessively thick, brittle shell can reduce the ability of the architecture to accommodate local plastic strain and may promote crack initiation within the shell or at the shell–matrix boundary. Conversely, a very thin shell may be insufficient to sustain high interfacial shear stresses or to provide effective shielding of the core. The optimal thickness is therefore architecture-dependent and must be selected together with shell composition, core ductility, reinforcement spacing, and matrix strength [64,65,68,69,78,79].

Shell composition is equally important because it determines the stiffness and hardness contrast, chemical compatibility, diffusion behavior, and deformation mode of the transition region. Carbide-rich shells such as NbC–Fe, TaC–Fe, and WC–Fe provide high hardness and efficient load transfer, whereas metallic-containing or graded regions reduce the abrupt mechanical mismatch between a hard carbide and the Fe matrix. In the W@WC/Fe architecture, the graded WC–Fe shell and ductile W core allow the reinforcement to carry high loads while retaining substantial fracture strain; the 2025 study reported a yield strength of 2326 ± 23 MPa together with a fracture strain of 23.6 ± 1.3% [65].

The composition gradient also influences interface stability. A gradual change from a metallic core to a carbide-rich shell and then to the Fe matrix can reduce local stress concentrations and suppress premature debonding. This principle is consistent with the measured hardness gradients in NbC–Fe and TaC–Fe shells and with the hierarchical WC–Fe architecture, where the shell acts as a transition region rather than as a simple barrier coating [64,68–70]. Thus, the design variable is not shell thickness alone but the coupled thickness–composition profile that determines how load is transferred, where plastic strain accumulates, and how cracks are deflected or arrested.

4.5. Current Challenges and Limitations

Despite significant progress in the development of architectured core–shell-reinforced Fe-based MMCs, several challenges remain before these materials can be widely implemented in practical engineering applications.

The first challenge is the complexity of fabrication processes and the reproducibility of core–shell architectures. Many reported systems require multiple processing steps, including infiltration, solid-state diffusion, laser processing, coating, or powder modification. Although these approaches enable precise control of interface characteristics, maintaining uniform shell thickness, chemical composition, and reinforcement distribution remains difficult, particularly during scale-up production [65,70–72].

A second challenge is the difficulty of large-scale manufacturing. Many core–shell structures have been demonstrated mainly at laboratory or small-batch scales, whereas industrial applications require stable, economical, and reproducible processing routes capable of producing large quantities of uniformly architectured reinforcements. Variations in shell morphology, interface structure, or reinforcement distribution may result in localized stress concentration and reduced mechanical reliability [65,72].

Another important limitation is the balance between shell hardness and damage tolerance. Highly ceramic- or carbide-rich shells provide excellent hardness and wear resistance but may introduce brittleness if the interface is not properly designed. The successful performance of Nb–NbC/Fe, Ta–TaC/Fe, and W–WC/Fe core–shell systems demonstrates that graded and hierarchical interfaces can partially overcome this limitation by combining hard reinforcement regions with tougher metallic transitions and improved stress accommodation [64,65,68–70].

Long-term service performance remains one of the least quantified aspects of core–shell-reinforced Fe-based MMCs. The available studies are dominated by quasi-static mechanical testing and short-duration wear experiments, whereas systematic data on fatigue, corrosion, and long-term thermal stability are still limited. This is particularly important because the high shell hardness and strong interfacial constraint that enhance static strength may also increase sensitivity to cyclic or environmentally assisted damage when pores, residual stresses, or local interfacial defects are present [57,64,68–70].

Among the available long-term-related properties, wear resistance is the most convincingly demonstrated. The W@WC/Fe core–shell composite showed a 234.2-fold improvement in wear resistance compared with cast iron, indicating that the graded WC–Fe shell and metallic W core can effectively stabilize the hard reinforcement against damage and spallation [65]. Evidence for thermal stability is also encouraging: W–WC/Fe composite fibers retained their characteristic core–shell architecture after treatment at 1145 °C for 18 h, while the refractory TaC phase provides high-temperature stability in Ta–TaC/Fe systems [69,70]. However, these results mainly demonstrate resistance under specific processing or laboratory conditions and should not yet be interpreted as evidence of long-term service durability.

In contrast, fatigue and corrosion performance remain insufficiently characterized. The reviewed studies do not provide a sufficiently consistent database of fatigue life or crack-growth behavior for establishing a quantitative fatigue advantage of core–shell architectures. Similarly, although preservation of the graded WC–Fe structure after hydrochloric-acid exposure has been reported [70], systematic corrosion-lifetime and corrosion–fatigue data are lacking. Further work should therefore evaluate fatigue, corrosion, thermal cycling, oxidation, and microstructural evolution under service-relevant conditions, with particular attention to the effects of shell thickness, interface morphology, residual stresses, and interdiffusion.

Finally, the relationship between processing parameters, interface evolution, and final mechanical properties requires deeper investigation. Advanced characterization techniques combined with computational modelling and data-driven approaches will be essential for establishing predictive relationships between core–shell architecture, processing conditions, and macroscopic performance.

4.6. Future Perspectives

Future development of architectured core–shell-reinforced Fe-based MMCs should move beyond empirical optimization of individual reinforcement systems toward a more systematic design strategy integrating interface engineering, advanced manufacturing, computational modelling, and data-driven materials discovery.

One promising direction is the development of functionally graded core–shell architectures, in which the chemical composition, mechanical properties, and structural characteristics gradually transition from the reinforcement core to the surrounding Fe matrix. Such graded interfaces can effectively reduce stress concentration, improve load transfer efficiency, and provide a better balance between strength, toughness, and ductility. Future research should therefore focus on precise control of shell thickness, compositional gradients, and interfacial phase evolution to achieve optimized mechanical performance.

Another important research direction is the integration of core–shell architectures with advanced manufacturing technologies, including additive manufacturing, laser-based processing, and digitally controlled fabrication approaches. These technologies provide new opportunities for producing complex reinforcement distributions, hierarchical interfaces, and spatially tailored mechanical responses. In particular, additive manufacturing may enable the fabrication of Fe-based MMC components with locally optimized reinforcement architectures that are difficult to achieve using conventional processing routes.

The integration of computational materials design and artificial intelligence (AI)-assisted optimization represents an important opportunity for accelerating the discovery and development of next-generation core–shell MMCs. High-throughput computational approaches can be employed to screen candidate reinforcement compositions, evaluate phase stability, and predict possible interfacial reactions before experimental validation. Such computational strategies have demonstrated considerable potential for accelerating materials discovery and reducing experimental optimization efforts [80].

Furthermore, machine-learning-based materials informatics provides powerful tools for establishing quantitative relationships between processing parameters, microstructural characteristics, interface structures, and mechanical properties. By combining experimental databases with computational simulations, machine-learning models can assist in predicting material performance and identifying optimized reinforcement architectures for specific engineering applications [81]. Recent advances in artificial intelligence-driven materials discovery further demonstrate the capability of data-driven approaches to identify promising material systems and processing conditions with reduced development time [82].

For architectured core–shell materials, AI-assisted approaches are particularly attractive because their mechanical behavior depends on multiple interacting structural parameters, including reinforcement topology, interface morphology, shell thickness, spatial distribution, and hierarchical organization. Recent progress in inverse design and computational optimization of architected materials provides new opportunities for developing core–shell structures with targeted deformation behavior and enhanced mechanical functionality [83]. Moreover, machine-learning models capable of predicting deformation mechanisms in architectured materials may provide valuable guidance for optimizing shell architectures and improving the reliability of Fe-based MMCs under complex loading conditions [84].

Future research should also extend evaluation criteria beyond conventional strength and hardness measurements. Practical applications require a comprehensive understanding of fatigue resistance, wear behavior, corrosion stability, thermal performance, and long-term structural reliability. Therefore, future core–shell MMC development should adopt multifunctional design principles, where mechanical performance is optimized together with environmental stability and service durability.

Finally, the transition of architectured core–shell Fe-based MMCs from laboratory-scale demonstrations to industrial applications requires scalable, cost-effective, and reproducible manufacturing strategies. The combination of advanced processing technologies, computational design, and AI-assisted optimization is expected to provide a pathway toward rationally designed metal matrix composites with controlled interfaces, predictable mechanical behavior, and application-oriented performance.

5. Conclusions

This review shows that the performance of Fe-based metal matrix composites is strongly influenced by the coupled effects of fabrication route, reinforcement architecture, microstructural evolution, and interface chemistry. Powder metallurgy provides effective control over particle distribution and densification; casting offers productivity and scalability for larger components; and additive manufacturing provides geometric flexibility together with opportunities for spatially tailored reinforcement and functionally graded structures.

Across these processing routes, conventional dispersed reinforcements may be affected by agglomeration, poor wetting, interfacial reactions, thermal mismatch, and defect formation. Architectured core–shell reinforcements introduce an additional design variable through control of the core–shell transition and can promote improved load transfer, stress redistribution, and damage tolerance while offering opportunities to balance strength, hardness, wear resistance, and ductility. The representative Nb–NbC/Fe, W@WC/Fe, V_8C_7/Fe, Ta–TaC/Fe, and W–WC/Fe systems reviewed in this work suggest that promising architectures generally combine hard strengthening regions with metallic or graded regions that accommodate deformation and support interface stability. At the same time, reproducible shell formation, scale-up, long-term service performance, and quantitative process–structure–property relationships remain important challenges.

Future progress will benefit from the combined development of feedstock and interface engineering, advanced manufacturing and post-processing, computational material design, and data-driven approaches. Particular attention should be given to functionally graded and hierarchical architectures, quantitative control of shell morphology and composition, and validation under cyclic, thermal, corrosive, and wear conditions relevant to engineering service. The integration of additive manufacturing, computational modelling, and artificial intelligence-assisted optimization may further support the development of architectured Fe-based MMCs with better-controlled interfaces and more predictable performance while helping to accelerate material and process optimization.

Author Contributions: Conceptualization, P.M.K. and E.G.Z.; methodology, P.M.K. and V.E.G.; formal analysis, V.K.K. and V.E.G.; writing—original draft preparation, P.M.K. and E.G.Z.; writing—review and editing, P.M.K., V.K.K. and E.G.Z.; visualization, P.M.K. and V.K.K.; funding acquisition, E.G.Z. All authors have read and agreed to the published version of the manuscript.

Funding: This work was supported by the Ministry of Science and Higher Education of the Russian Federation through the agreement no 075-15-2026-242, dated 28 April 2026.

Data Availability Statement: No new data were created or analyzed in this study. Data sharing is not applicable to this article.

Acknowledgments: During the preparation of this manuscript, the authors used ChatGPT (OpenAI, version GPT-5.6 Luna) for grammar improvement and proofreading. The authors have reviewed and edited the output and take full responsibility for the content of this publication.

Conflicts of Interest: The authors declare no conflicts of interest.

Abbreviations

The following abbreviations are used in this manuscript:

AM	Additive manufacturing
BJ	Binder jetting
CNTs	Carbon nanotubes
DED	Directed energy deposition
EBM	Electron beam melting
EB-PBF	Electron beam powder bed fusion
Fe-based MMCs	Iron-based metal matrix composites
FGM	Functionally graded materials
HDI strengthening	Hetero-deformation-induced strengthening
FS	Fracture strain
HIP	Hot Isostatic Pressing
LPBF	Laser powder bed fusion
ODS steel	Oxide-dispersion-strengthened steel
PM	Powder metallurgy
SLM	Selective laser melting
UCS	Ultimate compressive strength
UTS	Ultimate tensile strength
YS	Yield strength

References

1. Chen, S.; Chu, S.; Mao, B. Iron-Based Metal Matrix Composite: A Critical Review on the Microstructural Design, Fabrication Processes, and Mechanical Properties. *Acta Metall. Sin. (Engl. Lett.)* **2024**, *38*, 1–44. [CrossRef]
2. Singh, A.; Singh, J.; Sinha, M.K.; Kumar, R. Ferrous-Metal Matrix Composites: A Review on Status, Scope and Challenges. *Int. J. Interact. Des. Manuf. (IJIDeM)* **2023**, *17*, 2807–2829. [CrossRef]
3. Dong, W.; Yang, X.; Wang, K.; Liu, B. Research and Prospect of Particle Reinforced Iron Matrix Composites. *Int. J. Adv. Manuf. Technol.* **2023**, *128*, 3723–3744. [CrossRef]
4. Dharmalingam, G.; Sisodia, V.; Murali, A.P.; Naranje, V. Recent Advances in Development of Ferritic ODS Steel through Powder Metallurgy Route: A Comprehensive Overview. In *Powder Metallurgy: Characterization, Processing and Optimization Techniques*; Woodhead Publishing Reviews: Mechanical Engineering Series; Woodhead Publishing: Cambridg, UK, 2026; pp. 157–175. [CrossRef]
5. Wang, J.; Liu, S.; Xu, B.; Zhang, J.; Sun, M.; Li, D. Research Progress on Preparation Technology of Oxide Dispersion Strengthened Steel for Nuclear Energy. *Int. J. Extrem. Manuf.* **2021**, *3*, 032001. [CrossRef]
6. Singh, R.; Auger, M.A.; Kumar, D.; Prakash, U. A Critical Review of Consolidation Processes for ODS Steels: Development as Clad Tube Materials in Gen IV Nuclear Reactors. *Crit. Rev. Solid State Mater. Sci.* **2026**, *51*, 273–306. [CrossRef]
7. Oke, S.R.; Ige, O.O.; Falodun, O.E.; Okoro, A.M.; Mphahlele, M.R.; Olubambi, P.A. Powder Metallurgy of Stainless Steels and Composites: A Review of Mechanical Alloying and Spark Plasma Sintering. *Int. J. Adv. Manuf. Technol.* **2019**, *102*, 3271–3290. [CrossRef]
8. Murphy, C.; Buksa, S.; Day, J.; Felix-Lopez, A.; Antony Jose, S.; Menezes, P.L. Disruptive Manufacturing of Oxide Dispersion-Strengthened Steels for Nuclear Applications: Advances, Challenges, and Future Prospects. *Processes* **2025**, *13*, 1572. [CrossRef]
9. Nagini, M.; Murty, B.S. Mechanical Alloying: An Advanced Processing Route for Development of Iron Based Oxide Dispersion Strengthened Alloys. *Adv. Eng. Mater.* **2025**, *27*, 2401111. [CrossRef]
10. Wang, C.; Xiao, Y.; Zhang, W.; Zhao, T.; Du, H.; Li, Y. Achieving the Synergistic Strength and Wear Resistance in TiC/Fe Matrix Composites by Spark Plasma Sintering and Hot Isostatic Pressing. *J. Mater. Res. Technol.* **2025**, *36*, 7228–7243. [CrossRef]
11. García Díaz, C.; Benavidez, E.R.; García, J.L.; Brandaleze, E. Effect of Mechanical Milling on Powder Characteristics of Fe-Based Metal Matrix Composites Reinforced with WC–Co and NbC Particles. *MRS Adv.* **2024**, *9*, 78–82. [CrossRef]
12. Tripathi, M.K.; Singh, V.B. Microstructure and Properties of Si_3N_4 and TiN Nano-Particles Reinforced Electrodeposited Functional Ni-Fe Matrix Nanocomposite. *J. Electrochem. Soc.* **2016**, *163*, D453. [CrossRef]
13. Liu, J.; Ding, R.; Cao, J.; Zhan, K.; Li, S.; Zhao, B.; Ji, V. Recent Progress in Architecture Design of Nanocarbon-Reinforced Metal Matrix Composites and Their Properties: A Review. *Carbon* **2024**, *228*, 119382. [CrossRef]
14. Meher, B.S.; Chaira, D. Effect of MWCNTs Content and Sintering Atmosphere on Microstructure and Various Properties of Iron MWCNTs MMC Fabricated by Conventional Powder Metallurgy. *Diam. Relat. Mater.* **2025**, *153*, 112086. [CrossRef]

15. Gutema, E.M.; Lemu, H.G. Conventional Machining of Metal Matrix Composites towards Sustainable Manufacturing—Present Scenario and Future Prospects. *J. Compos. Sci.* **2024**, *8*, 356. [CrossRef]
16. Xu, M.; Ren, K.; Chen, L.; Xu, X.; Xue, Y.; Li, H.; Ma, Y.; Weng, D.; Lv, Z.; Tang, P.; et al. Friction and Wear Characteristics of Iron Based Composites Fabricated by Hot Isostatic Pressing. *J. Mater. Sci.* **2025**, *60*, 19695–19712. [CrossRef]
17. Zemtsova, E.G.; Arbenin, A.Y.; Sidorov, Y.V.; Morozov, N.F.; Korusenko, P.M.; Semenov, B.N.; Smirnov, V.M. The Use of Carbon-Containing Compounds to Prepare Functional and Structural Composite Materials: A Review. *Appl. Sci.* **2022**, *12*, 9945. [CrossRef]
18. Zemtsova, E.G.; Yurchuk, D.V.; Smirnov, V.M. Creation of heterogeneity on the basis of carbide nanostructures in the volume of metal (iron) matrix for regulation of mechanical properties. *Mater. Phys. Mech.* **2013**, *18*, 42–52.
19. Zemtsova, E.G.; Yurchuk, D.V.; Sidorov, Y.V.; Semenov, B.N.; Morozov, N.F.; Smirnov, V.M. Synthesis of metallic composite based on iron frame and SiC nanostructures and its strength properties. *Mater. Phys. Mech.* **2020**, *46*, 122–131.
20. Zemtsova, E.; Yurchuk, D.; Smirnov, V. The Process of Nanostructuring of Metal (Iron) Matrix in Composite Materials for Directional Control of the Mechanical Properties. *Sci. World J.* **2014**, *2014*, 979510. [CrossRef] [PubMed]
21. Pagounis, E.; Lindroos, V.K.; Talvitie, M. Influence of Matrix Structure on the Abrasion Wear Resistance and Toughness of a Hot Isostatic Pressed White Iron Matrix Composite. *Metall. Mater. Trans. A* **1996**, *27*, 4183–4191. [CrossRef]
22. Sankhla, A.M.; Patel, K.M.; Makhesana, M.A.; Giasin, K.; Pimenov, D.Y.; Wojciechowski, S.; Khanna, N. Effect of Mixing Method and Particle Size on Hardness and Compressive Strength of Aluminium-Based Metal Matrix Composite Prepared through Powder Metallurgy Route. *J. Mater. Res. Technol.* **2022**, *18*, 282–292. [CrossRef]
23. Sueyoshi, H.; Maruno, T.; Yamamoto, K.; Hirata, Y.; Sameshima, S.; Uchida, S.; Hamauzu, S.; Kurita, S. Processing of Continuous Ceramic Fiber/Iron Alloy Composite by Powder Metallurgy. *J. Jpn. Inst. Met. Mater.* **2001**, *65*, 961–968. [CrossRef]
24. Naji, K.; Marinova, M.; Touzin, M.; Pouligny, P.; Avettand-Fènoël, M.N. Design and Characterization of an Oxides Hybrid Dispersion Strengthened Iron Based Composite with a Graded and Architectural Microstructure. *J. Alloys Compd.* **2019**, *802*, 217–228. [CrossRef]
25. Pribytkov, G.A.; Baranovskiy, A.V.; Firsina, I.A.; Akimov, K.O.; Krivopalov, V.P. Study of Fe-Matrix Composites with Carbide Strengthening, Formed by Sintering of Iron Titanides and Carbon Mechan-ically Activated Mixtures. *Obrab. Met.-Met. Work. Mater. Sci.* **2024**, *26*, 212–223. [CrossRef]
26. Fansteel Metallurgical Corp. Dispersion Strengthened Iron Group Metal Alloyed with a Small Amount of Zirconium, Hafnium or Magnesium and Process of Making. U.S. Patent 3,382,051, 7 May 1968.
27. Tokova, L.V.; Zaitsev, A.A.; Kurbatkina, V.V.; Levashov, E.A.; Sidorenko, D.A.; Andreev, V.A. The features of influence of ZrO_2 and WC nanodispersed additives on the properties of metal matrix composite. *Russ. J. Non-Ferr. Met.* **2014**, *55*, 186–190. [CrossRef]
28. Gierl-Mayer, C. Reactions between ferrous powder compacts and atmospheres during sintering – an overview. *Powder Metall.* **2020**, *63*, 238–249. [CrossRef]
29. Malik, A.R.; Pani, B.B.; Badjena, S.K. Powder Metallurgy Processed Ferrous Composites: A Review. *Int. J. Eng. Adv. Technol. (IJEAT)* **2017**, *6*, 12–15.
30. Ceschini, L.; Morri, A.; Rotundo, F. Forming of Metal Matrix Composites. In *Comprehensive Materials Processing*; Elsevier: Amsterdam, The Netherlands, 2014; Volume 3, pp. 159–186. [CrossRef]
31. Ren, P.; Ouyang, Y.; Mu, J.; Luo, S.; Tang, Z.; Wu, Y.; Leung, C.L.A.; Oliveira, J.P.; Zou, Y.; Wang, H.; et al. Metal Powder Atomization Preparation, Modification, and Reuse for Additive Manufacturing: A Review. *Prog. Mater. Sci.* **2025**, *152*, 101449. [CrossRef]
32. Ramanathan, A.; Krishnan, P.K.; Muraliraja, R. A Review on the Production of Metal Matrix Composites through Stir Casting—Furnace Design, Properties, Challenges, and Research Opportunities. *J. Manuf. Process.* **2019**, *42*, 213–245. [CrossRef]
33. Adediran, A.A.; Ogunkola, A.B.; Edoziuno, F.O.; Adesina, O.S.; Saravana Kumar, M.; Okechukwu, O.C. Squeeze Casting Process: Trends and Opportunities. In *Casting Processes*; IntechOpen: London, UK, 2022. [CrossRef]
34. Vijayaram, T.R. Advances in Squeeze Casting Technique for Processing Discontinuous Ceramic Fibre Reinforced Metal Matrix Composite Materials. *INTI J.* **2006**, *2*, 649–654.
35. Mishra, R.R.; Sahoo, A.K.; Panda, A.; Kumar, R. Machinability of Ultrasonic-Stir-Squeeze Cast A356/ZrO_2/GO Hybrid Nanocomposite under Sustainable MQL Condition. *Proc. Inst. Mech. Eng. Part E J. Process Mech. Eng.* **2025**, 09544089251409243. [CrossRef]
36. Sethy, P.; Poddar, P.; Sahoo, A.K.; Kumar, R.; Panda, A.; Das, D. Synthesis, Characterization and Machinability Investigation of Novel Ultrasonically Aided Stir-Squeeze Cast Al 7075/Fe-Cr Slag Nanocomposite and Squeeze Cast Unreinforced Al 7075 Alloy: Comparative Assessment. *Measurement* **2026**, *260*, 119811. [CrossRef]
37. Soni, S.K.; Thomas, B. Microstructure, Mechanical Properties and Machinability Studies of Al7075/SiC/h-BN Hybrid Nanocomposite Fabricated via Ultrasonic-Assisted Squeeze Casting. *FME Trans.* **2020**, *48*, 532–542. [CrossRef]
38. Gu, H.; Nakae, H. Spontaneous Infiltration Rate of SiCp/Cast Iron Composites. *J. Jpn. Foundry Eng. Soc.* **2004**, *76*, 909–914. [CrossRef]

39. Nakae, H.; Gu, H.; Wu, S. Fabrication of MMCs by Spontaneous Infiltration of Cast Iron Melt into SiCp Preform. *J. Jpn. Foundry Eng. Soc.* **2004**, *76*, 296–302. [CrossRef]
40. Avand, R.; Ghaderi Hamidi, A.; Pourabdoli, M. Feasibility of Production of an Iron Base Metal Matrix Composite by Infiltration of Molten Gray Cast Iron into a 304 Stainless Steel Porous Skeleton. *J. Sci. Technol. Compos.* **2022**, *8*, 1653–1658. [CrossRef]
41. Fang, Y.; Kim, M.K.; Zhang, Y.; Duan, Z.; Yuan, Q.; Suhr, J. Particulate Reinforced Iron Based Metal Matrix Composites Fabricated by Selective Laser Melting: A Systematic Review. *J. Manuf. Process.* **2022**, *74*, 592–639. [CrossRef]
42. Zheng, Q.; Yin, Y.; Lu, C.; Cui, X.; Gao, Y.; Zhu, H.; Li, Z.; Shi, J.; Shi, W.; Tie, D. Research Progress on Laser Additive Manufacturing of Oxide Dispersion-Strengthened Alloys—A Review. *Materials* **2025**, *18*, 4094. [CrossRef] [PubMed]
43. Ansari, P.; Rehman, A.U.; Pitir, F.; Veziroglu, S.; Mishra, Y.K.; Aktas, O.C.; Salamci, M.U. Selective Laser Melting of 316L Austenitic Stainless Steel: Detailed Process Understanding Using Multiphysics Simulation and Experimentation. *Metals* **2021**, *11*, 1076. [CrossRef]
44. Nartu, M.; Agrawal, P. Additive Manufacturing of Metal Matrix Composites. *Mater. Des.* **2025**, *252*, 113609. [CrossRef]
45. Ansari, M.; Jabari, E.; Toyserkani, E. Opportunities and Challenges in Additive Manufacturing of Functionally Graded Metallic Materials via Powder-Fed Laser Directed Energy Deposition: A Review. *J. Mater. Process. Technol.* **2021**, *294*, 117117. [CrossRef]
46. Perminov, A.; Jurisch, M.; Bartzsch, G.; Biermann, H.; Weißgärber, T.; Volkova, O. Manufacturing Fe–TiC metal matrix composite by Electron Beam Powder Bed Fusion from pre-alloyed gas atomized powder. *Mater. Sci. Eng. A* **2021**, *813*, 141130. [CrossRef]
47. Chen, Y.; Fu, Z.; Ye, J.; Wahlmann, B.; Körner, C. Additive Manufacturing of TiC/Steel Composites Using Electron Beam Melting and In Situ Infiltration. *Adv. Eng. Mater.* **2024**, *26*, 2301313. [CrossRef]
48. Shi, Y.; Gong, S.; Xu, H.; Yang, G.; Qiao, J.; Wang, Z.; Zhang, J.; Qi, B. Electron beam metal additive manufacturing: Defects formation and in-process control. *J. Manuf. Process.* **2023**, *101*, 386–431. [CrossRef]
49. Li, M.; Du, W.; Elwany, A.; Pei, Z.; Ma, C. Metal Binder Jetting Additive Manufacturing: A Literature Review. *J. Manuf. Sci. Eng.* **2020**, *142*, 090801. [CrossRef]
50. Ostolaza, M.; Arrizubieta, J.I.; Lamikiz, A.; Plaza, S.; Ortega, N. Latest Developments to Manufacture Metal Matrix Composites and Functionally Graded Materials through AM: A State-of-the-Art Review. *Materials* **2023**, *16*, 1746. [CrossRef] [PubMed]
51. Ye, C.; Zhang, C.; Zhao, J.; Dong, Y. Effects of Post-processing on the Surface Finish, Porosity, Residual Stresses, and Fatigue Performance of Additive Manufactured Metals: A Review. *J. Mater. Eng. Perform.* **2021**, *30*, 6407–6425. [CrossRef] [PubMed]
52. Yu, H.; Xin, Y.; Wang, M.; Liu, Q. Hall-Petch Relationship in Mg Alloys: A Review. *J. Mater. Sci. Technol.* **2018**, *34*, 248–256. [CrossRef]
53. Liang, G.F.; Liu, Y.G.; Yang, X.L.; Tan, Q.Y.; Wu, T.; Wang, J.J.; Atrens, A.; Tian, Z.Q.; Zhang, M.X. Refinement of cast microstructure of A517 steel by addition of TiB2. *J. Iron Steel Res. Int.* **2024**, *31*, 2815–2827. [CrossRef]
54. Akhtar, F. Ceramic Reinforced High Modulus Steel Composites: Processing, Microstructure and Properties. *Can. Metall. Q.* **2014**, *53*, 253–263. [CrossRef]
55. Liu, J.; Li, Y.-L.; Li, A.-M.; Yang, H.-Y.; Dong, B.-X.; Zhong, X.-M.; Wang, C.-G.; Li, Z.-G.; Chen, D.-L.; Yu, Y.; et al. Preparation of Iron-Based Composites Reinforced with Submicron/Nano-Sized TiC Ceramic Particles by In-Situ Reaction in Melts and One-Step Integrated Hot Pressing Densification. *Ceram. Int.* **2025**, *51*, 4400–4411. [CrossRef]
56. Wu, T.T.; Wang, H.M.; Li, G.R.; Chou, S.S.; Zhao, B.W. Study on the Microstructure and Performance of FeCoNiCrMn High-Entropy Alloy-Based Composites Reinforced by Nano-Al_2O_3 Particles. *J. Mater. Res. Technol.* **2025**, *35*, 3751–3762. [CrossRef]
57. Hebert, R.J. Viewpoint: Metallurgical Aspects of Powder Bed Metal Additive Manufacturing. *J. Mater. Sci.* **2016**, *51*, 1165–1175. [CrossRef]
58. DebRoy, T.; Wei, H.L.; Zuback, J.S.; Mukherjee, T.; Elmer, J.W.; Milewski, J.O.; Beese, A.M.; Wilson-Heid, A.; De, A.; Zhang, W. Additive Manufacturing of Metallic Components–Process, Structure and Properties. *Prog. Mater. Sci.* **2018**, *92*, 112–224. [CrossRef]
59. Miracle, D.B. Metal Matrix Composites—From Science to Technological Significance. *Compos. Sci. Technol.* **2005**, *65*, 2526–2540. [CrossRef]
60. Clyne, T.W.; Withers, P.J. *An Introduction to Metal Matrix Composites*; Cambridge University Press: Cambridge, UK, 1993. [CrossRef]
61. Dudina, D.V.; Georgarakis, K. Core–Shell Particle Reinforcements—A New Trend in the Design and Development of Metal Matrix Composites. *Materials* **2022**, *15*, 2629. [CrossRef] [PubMed]
62. Chawla, N.; Chawla, K.K. *Metal Matrix Composites*, 2nd ed.; Springer: New York, NY, USA, 2013. [CrossRef]
63. Lei, C.X.; Pan, Y.; Kuang, F.; Huo, W.T.; Zhu, M.; Lu, X. A Novel Configuration Design of Strong and Ductile (TiC + Ti_5Si_3)/Ti Laminated Composites. *Mater. Sci. Eng. A* **2024**, *892*, 145961. [CrossRef]
64. Bai, H.; Zhong, L.; Kang, L.; Wei, J.; Lv, Z.; Xu, Y. A Novel Iron Matrix Composite Fabricated by Two-Step In Situ Reaction: Microstructure, Formation Mechanism and Mechanical Properties. *J. Alloys Compd.* **2021**, *855*, 157442. [CrossRef]
65. Bai, H.; Yang, T.; Wang, L.; Kang, L.; He, M.; Zhuang, W.; Zhong, L.; Wan, Z.; Xu, Y. Achieving Concurrent Strength-Ductility Combination and Robust Anti-Wear Performance in W@WC/Fe Core-Shell Bar-Reinforced Iron Matrix Composites. *Mater. Sci. Eng. A* **2025**, *931*, 148189. [CrossRef]

66. Bai, H.; Zhong, L.; Cui, P.; Shang, Z.; Lv, Z.; Xu, Y. Microstructure and Compressive Properties of V_8C_7/Fe Core-Shell Rod-Reinforced Iron-Based Composite Fabricated via Two-Step In-Situ Reaction. *Vacuum* **2020**, *176*, 109302. [CrossRef]
67. Kou, B.H.; Lu, D.; Gong, W.; Wei, S.; Jiang, C. Compressive and Wear Properties of Al_2O_3/High Manganese Steel Composites with a Spatial Lattice Architecture. *Mater. Today Commun.* **2022**, *32*, 104159. [CrossRef]
68. Zhong, L.; Bai, H.; Wei, J.; Zhu, J.; Peng, J.; Lu, Z.; Xu, Y. In Situ Fabricated Metal-Carbide with Core-Shell Structure for High Impact-Toughness Iron-Matrix Composite. *Mater. Sci. Technol.* **2019**, *35*, 1727–1734. [CrossRef]
69. Bai, H.; Zhong, L.; Shang, Z.; Xu, Y.; Wu, H.; Bai, J.; Cao, B.; Wei, J. Microstructure and Impact Properties of Ta-TaC Core-Shell Rod-Reinforced Iron-Based Composite Fabricated by In Situ Solid-Phase Diffusion. *J. Alloys Compd.* **2018**, *768*, 340–348. [CrossRef]
70. Bai, H.; Kang, L.; Zhuang, W.; Liu, J.; Zhong, L.; Xu, Y. Microstructure and Mechanical Properties of W-WC/Fe Composite Fiber-Reinforced Fe Matrix Composite Prepared by Combination of Infiltration and In-Situ Solid Phase Diffusion. *J. Mater. Res. Technol.* **2023**, *27*, 5305–5314. [CrossRef]
71. Ma, J.; Wu, X.; Wang, Z.; Li, L.; Guo, F. Microstructure and Mechanical Properties of Fe-Based Composite Coatings Reinforced with In-Situ Synthesized Multilayer Core-Shell Al_2O_3@TiC@TiB Ceramic Particles via Laser Cladding. *Appl. Surf. Sci.* **2026**, *715*, 164528. [CrossRef]
72. Wang, Z.; Tan, M.; Wang, J.; Zeng, J.; Zhao, F.; Xiao, X.; Xu, S.; Liu, B.; Gong, L.; Sui, Q.; et al. Core-Shell Structural Iron Based Metal Matrix Composite Powder for Laser Cladding. *J. Alloys Compd.* **2021**, *878*, 160127. [CrossRef]
73. Xiong, X.; Liu, Y.; Wang, R.; Deng, X.; Li, Y.; Ping, E.; Yang, S. The Microstructure and Properties of Novel TiO_2@WC Core–Shell Reinforced 316 Stainless Steel Composite Prepared by SLM. *Mater. Lett.* **2025**, *398*, 138980. [CrossRef]
74. Li, H.; Hu, Y.; Di, R.; Yuan, R.; Shi, C.; Lei, J. Effects of WC Particles on Microstructure and Mechanical Properties of 316L Steel Obtained by Laser Melting Deposition. *Ceram. Int.* **2022**, *48*, 20388–20399. [CrossRef]
75. Sahoo, C.K.; Masanta, M. Microstructure and Mechanical Properties of TiC-Ni Coating on AISI304 Steel Produced by TIG Cladding Process. *J. Mater. Process. Technol.* **2017**, *240*, 126–137. [CrossRef]
76. Ouyang, J.H.; Li, X.; Lei, T.C. Electron Microscopy Structure Study of Laser-Clad TiC-Ni Particle-Reinforced Coating. *J. Mater. Eng. Perform.* **2000**, *9*, 234–246. [CrossRef]
77. Li, H.; Song, Q.; Xu, Q.; Chen, Y.; Xu, L.; Man, T. Electrochemical Synthesis of Core-Shell-Structured NbC-Fe Composite Powder for Enforcement in Low-Carbon Steel. *Materials* **2017**, *10*, 1257. [CrossRef] [PubMed]
78. Zhong, L.; Wei, J.; Bai, H.; Zhu, J.; Xu, Y. Effects of Soaking Time on the Microstructure and Mechanical Properties of Nb–NbC/Fe Core–Shell Rod-Reinforced Cast-Iron-Matrix Composite Fabricated through Two-Step In Situ Solid-Phase Diffusion. *J. Mater. Res. Technol.* **2020**, *9*, 12308–12317. [CrossRef]
79. Bai, H.; Wang, L.; Kang, L.; Liu, J.; Zhuang, W.; Zhong, L.; Wan, Z.; Xu, Y. Microstructure and Mechanical Properties Evolution of W@WC/Fe Core–Shell Bar-Reinforced Iron Matrix Composites: Effect of In-Situ Solid Diffusion Time. *Adv. Eng. Mater.* **2024**, *26*, 2400967. [CrossRef]
80. Curtarolo, S.; Hart, G.L.W.; Nardelli, M.B.; Mingo, N.; Sanvito, S.; Levy, O. The high-throughput highway to computational materials design. *Nat. Mater.* **2013**, *12*, 191–201. [CrossRef] [PubMed]
81. Ramprasad, R.; Batra, R.; Pilania, G.; Mannodi-Kanakkithodi, A.; Kim, C. Machine learning in materials informatics: Recent applications and prospects. *npj Comput. Mater.* **2017**, *3*, 54. [CrossRef]
82. Butler, K.T.; Davies, D.W.; Cartwright, H.; Isayev, O.; Walsh, A. Machine learning for molecular and materials science. *Nature* **2018**, *559*, 547–555. [CrossRef] [PubMed]
83. Jiao, P.; Mueller, J.; Raney, J.R.; Zheng, X.; Alavi, A.H. Mechanical metamaterials and beyond. *Nat. Commun.* **2023**, *14*, 6004. [CrossRef] [PubMed]
84. Karapiperis, K.; Kochmann, D.M. Prediction and control of fracture paths in disordered architected materials using graph neural networks. *Commun. Eng.* **2023**, *2*, 32. [CrossRef]

Disclaimer/Publisher's Note: The statements, opinions and data contained in all publications are solely those of the individual author(s) and contributor(s) and not of MDPI and/or the editor(s). MDPI and/or the editor(s) disclaim responsibility for any injury to people or property resulting from any ideas, methods, instructions or products referred to in the content.